

ISOLATING NEIGHBORHOOD TRAJECTORY COMPUTATIONS IN NON-AUTONOMOUS SYSTEMS INCLUDING THE ELLIPTIC RESTRICTED THREE-BODY PROBLEM

Rodney L. Anderson,^{*} Robert W. Easton,[†] and Martin W. Lo^{*}

Isolating block and isolating neighborhood methods have previously been implemented to find transit trajectories and orbits around libration points in the autonomous circular restricted three-body problem. For some applications, the direct computation of these types of trajectories in non-autonomous models more closely approximating real-world ephemerides is beneficial. Here, we apply isolating neighborhood methods to non-autonomous systems, including the elliptic restricted three-body problem (ERTBP). Specifically, simplified isolating neighborhood boundaries are computed around libration points in the ERTBP. These boundaries are used in combination with a bisection method to compute the forward asymptotic trajectories of the isolated invariant set and track orbits around a libration point.

LEAD PARAGRAPH

The computation of transit trajectories and orbits around libration points in the autonomous circular restricted three-body problem (CRTBP) has previously been enabled with the use of isolating blocks and isolating neighborhoods. The implementation of these methods in non-autonomous systems allows for a more straight-forward application of these algorithms to real-world models, although their use with non-autonomous systems presents several challenges. We address these issues by implementing new techniques in the non-autonomous elliptic restricted three-body problem. Specifically, the required boundaries are tested across a range of energies that span the potential energies that trajectories used in the computations may have, and the orbit tracking algorithm is adapted to perform corrections at any required time. The use of these methods allows the tracking of quasiperiodic orbits having the characteristics of 2-tori and 3-tori in the ERTBP.

INTRODUCTION

Isolating block and isolating neighborhood methods have previously been used to describe the dynamics near libration points in the circular restricted three-body problem (CRTBP).¹⁻⁴ Isolating blocks have been used to compute forward asymptotic trajectories approaching the L_2 isolated invariant set and closely track periodic and quasiperiodic orbits within the isolated invariant set.^{5,6} Isolating neighborhoods were then used to simplify the computations and compute trajectories closely tracking periodic and quasiperiodic orbits at higher energies including the halo orbit and quasi-halo orbit families.⁷ Another approach was introduced to compute desired periodic and

^{*}Technologist, Jet Propulsion Laboratory, California Institute of Technology, 4800 Oak Grove Drive, M/S 301-121, Pasadena, CA 91109

[†]Professor Emeritus, Applied Mathematics, University of Colorado at Boulder, Boulder, CO 80309

© 2023 California Institute of Technology. Government sponsorship acknowledged.

quasiperiodic orbits within the L_2 Lyapunov orbit in a surface of section directly without using asymptotic approach trajectories.⁸ This method also allows the computation of trajectories within the chaotic region in this surface of section.⁹ While the ability to compute these asymptotic trajectories in the autonomous CRTBP is very useful, our recent analyses have shown that it is possible to extend the isolating neighborhood methods used for the CRTBP to non-autonomous systems.

In this study, we extend our methods, previously developed for use in the autonomous CRTBP, to non-autonomous problems, including the elliptic restricted three-body problem (ERTBP). The isolating neighborhood boundaries developed for use in the CRTBP may be used as a starting point for computing analogous isolating neighborhood boundaries in the ERTBP. In the CRTBP, a chosen boundary may be checked to determine whether it is an isolating block boundary for a selected region by computing tangent trajectories at a particular Jacobi constant and integrating them forward and backward in time.⁷ In the ERTBP, there is no longer a Jacobi constant, but a similar boundary may be computed around regions such as the L_2 point.

In order to find an isolating neighborhood, we first specify a closed set B in phase space around a region of interest, in this case the region around the L_2 point. The closed set B is a manifold with two boundary components - a “right” and a “left” boundary. We verify the exit behavior of orbits to check that those that are tangent to the right boundary exit through the right boundary and orbits tangent to the left boundary exit left. In this case, the isolating neighborhood boundary for the ERTBP must be checked at various epochs to ensure that it remains an isolating neighborhood boundary for each epoch. While checking the tangent trajectories at each epoch, velocities must be computed for the tangent trajectories. Since the Jacobi constant does not exist in the ERTBP, a range of velocity magnitudes may be used to provide evidence that this boundary still works as an isolating boundary in the non-autonomous system.

Our approach using isolating neighborhoods serves as an alternative to standard approaches that typically use some combination of expansions and differential correction to compute quasiperiodic orbits in multibody systems. In the autonomous CRTBP, methods such as Fourier approaches,^{10,11} Lindstedt-Poincaré methods,¹² parameterization methods,^{13,14} normal form or semianalytical methods,^{15,16} Poincaré maps,^{17,18} and stroboscopic maps in combination with collocation^{19–22} have been used to compute quasiperiodic orbits. Although much of the work in the non-autonomous ERTBP has focused on the computation of periodic orbits,^{23–32} some work has been done to explore quasiperiodic tori in the ERTBP and other non-autonomous systems. More specifically, Capinski and Zgliczyński³³ examined the effect of perturbations in the planar ERTBP on Lyapunov orbits for small eccentricities and showed that these orbits are perturbed to quasiperiodic invariant tori. Kumar, Anderson, and de la Llave explored resonant tori in the planar ERTBP.^{34,35} Farres and Jorba³⁶ explored orbits within the elliptic Hill problem, and Jorba, Jorba-Cusó, and Rosales^{37,38} and Jorba and Villanueva 1997³⁹ studied the bicircular problem. More recently, Fernández, Haro, and Mondelo studied quasiperiodic orbits in the ERTBP.⁴⁰

In this paper, the isolating neighborhood boundaries are computed for a range of epochs and velocities. The implementation of bisection methods for the computation of the asymptotic trajectories approaching the isolated invariant set in the ERTBP is also discussed. To provide insight into these trajectories, we introduce several ERTBP coordinate systems. We first describe an ERTBP model using the standard constantly rotating coordinate system that is used to study the CRTBP.⁴¹ We also use a non-uniformly rotating system with an axis that remains aligned with the primaries,^{42–44} and finally, the commonly used ERTBP system with a non-uniformly rotating and pulsating frame.⁴⁵ Tracking methods for following periodic and quasiperiodic orbits within the isolated invariant set

are also developed and used to compute quasiperiodic orbits in the ERTBP. The resulting orbits are described and compared to results from the CRTBP.

MODELS

The previous analyses using isolating blocks and isolating neighborhoods have focused on computations within the CRTBP. Once the primaries are allowed to move in orbits of non-zero eccentricity, the complexity of the problem increases significantly, and the use of different ERTBP models is useful to aid in both computations and visualization of the results. Four different models are introduced and described here. The standard CRTBP is described first, followed by an ERTBP model with a constantly rotating frame, an ERTBP model with a non-uniformly rotating coordinate frame, and finally an ERTBP model with both a non-uniformly rotating and pulsating coordinate frame.

Circular Restricted Three-Body Problem

While the primary focus of this work is on computing orbits within the ERTBP, it is useful to compare the results to the orbits computed within the CRTBP. In the CRTBP, the motion of a point mass is computed in a rotating frame aligned with the primary and secondary masses which are constrained to move on circular orbits. The primary mass (the Earth for this study) is located on the rotating x axis at $E_{em} = (-\mu, 0, 0)$, while the secondary mass (the Moon) is located on the x axis at $M_{em} = (\lambda, 0, 0)$ where $\lambda = 1 - \mu$. The dimensionless mass $\mu = m_2/(m_1 + m_2)$ is defined where m_1 is the mass of the primary, and m_2 is the mass of the secondary. The equations of motion in this model are

$$\begin{aligned}\ddot{x} &= \partial_x \Phi(x, y, z) + 2\dot{y} \\ \ddot{y} &= \partial_y \Phi(x, y, z) - 2\dot{x} \\ \ddot{z} &= \partial_z \Phi(x, y, z)\end{aligned}\tag{1}$$

where

$$\Phi(x, y, z) = \frac{1}{2}(x^2 + y^2) + U(x, y, z)\tag{2}$$

and

$$U(x, y, z) = \lambda/r_1(x, y, z) + \mu/r_2(x, y, z).\tag{3}$$

Computing the partials gives

$$\begin{aligned}\ddot{x} &= 2\dot{y} + x - \frac{(x + \mu)(1 - \mu)}{r_1^3} - \frac{\mu(x - 1 + \mu)}{r_2^3} \\ \ddot{y} &= -2\dot{x} + y \left[1 - \frac{1 - \mu}{r_1^3} - \frac{\mu}{r_2^3} \right] \\ \ddot{z} &= z \left[-\frac{1 - \mu}{r_1^3} - \frac{\mu}{r_2^3} \right].\end{aligned}\tag{4}$$

The distance between the point mass and the primary is $r_1(x, y, z)$, and the distance from the point mass to the secondary is $r_2(x, y, z)$. This study focused on the Earth-Moon system using a mass ratio of $\mu = 1.2150584270571545 \times 10^{-2}$. A constant of motion (the Jacobi constant) exists in the CRTBP, and it is defined as $C = -2J$ where

$$J = \frac{1}{2} \langle \dot{q}, \dot{q} \rangle - \Phi(q)\tag{5}$$

or

$$C = -\dot{x}^2 - \dot{y}^2 - \dot{z}^2 + x^2 + y^2 + \frac{2(1-\mu)}{r_1} + \frac{2\mu}{r_2}. \quad (6)$$

Elliptic Restricted Three-Body Problem

One of the most common formulations of the ERTBP⁴⁵ uses a non-uniformly rotating coordinate system where the x axis is aligned with the primaries, and the length unit is chosen to be the varying distance between the primary and the secondary. The foundation for deriving the equations of motion for this system is laid here by first deriving the equations of motion in both uniformly and non-uniformly rotating coordinate systems. A new derivation for the non-uniformly rotating and pulsating coordinate system is then described. This results in the same equations of motion obtained using Szebehely's⁴⁵ derivation based on the work by Scheibner,⁴⁶ Petr and Nechvile,⁴⁷ Nechvile,⁴⁸ and Rein.⁴⁹

In the following, capital letters are used for inertial coordinates. Starting with the full three-body problem and making the third mass zero gives the equations of motion for a restricted three-body problem as

$$\ddot{Q}_1 = Gm_2|Q_2 - Q_1|^{-3}(Q_2 - Q_1) \quad (7)$$

$$\ddot{Q}_2 = Gm_1|Q_2 - Q_1|^{-3}(Q_1 - Q_2) \quad (8)$$

$$\ddot{Q}_3 = Gm_1|Q_1 - Q_3|^{-3}(Q_1 - Q_3) + Gm_2|Q_2 - Q_3|^{-3}(Q_2 - Q_3). \quad (9)$$

In these equations, Q is position, and V is velocity. The subscripts 1, 2, and 3 correspond to the primary, the secondary, and the infinitesimal mass, respectively. G is the universal gravitational constant, and the masses m_1 and m_2 are defined as they are in the CRTBP. Next, set the center of mass $m_1Q_1 + m_2Q_2 = 0$. Now, set $K = Gm_1 + Gm_2$ and define $\mu = Gm_2/K$ as in the CRTBP. Equations 7 and 8 decouple from Equation 9 and can be combined as Kepler's equation:

$$\ddot{Q}^* = -K|Q^*|^{-3}Q^*. \quad (10)$$

If $Q^*(t)$ is a solution of Equation 10 then $Q_1^*(t) = -\mu Q^*(t)$ and $Q_2^*(t) = (1-\mu)Q^*(t)$ are solutions of Equations 7 and 8.

To derive a model for the ERTBP one chooses the eccentricity e and the semi-major axis a for the ellipse $r(\nu) = \frac{a(1-e^2)}{1+e\cos(\nu)}$. Then one solves for initial conditions for a solution $Q^*(t)$ of Equation 10 that traverses the ellipse. Set $Q_1^*(t) = \mu Q^*(t)$ and $Q_2^*(t) = (1-\mu)Q^*(t)$. Then with Q_3 replaced by Q , the elliptic model is given by the equation

$$\ddot{Q} = Gm_1|Q_1^* - Q|^{-3}(Q_1^* - Q) + Gm_2|Q_2^* - Q|^{-3}(Q_2^* - Q). \quad (11)$$

Elliptic parameters for a solution of Kepler's Equation 10 are related to the semi-major axis a , the energy E , and angular momentum σ of the solution. Using the relations $e = \sqrt{1 + 2E\sigma^2/K^2}$ and $a(1-e^2) = \sigma^2/K$ one can choose initial conditions for a solution (Q^*, \dot{Q}^*) of Equation 11 that traverses the ellipse. We choose the initial conditions $Q^*(0) = [a(1-e); 0, 0]$ and $\dot{Q}^*(0) = [0; \sqrt{\frac{K(1+e)}{a(1-e)}}; 0]$. A normalized distance unit can be set so that $a(1-e) = 1$. For this unit, $Q^*(0) = [1; 0; 0]$ and $\dot{Q}^*(0) = [0; \sqrt{K(1+e)}; 0]$. Alternately one may set $a = 1$. The CRTBP model results from the choice $e = 0$. A hyperbolic "fly-by" model results from the choice $e > 1$.

Uniformly Rotating ERTBP Coordinate System

A formulation of the ERTBP using a coordinate frame with fixed rotation was introduced by Easton.⁴¹ This coordinate frame allows an easier comparison with the CRTBP since it uses the same frame. Both the primary and secondary will move in position in this frame. We will refer to Easton for the detailed derivation, but an overview is given here.

The CRTBP is derived when a circular solution $Q^*(t)$ of radius a of Kepler's equation is chosen, and a constantly rotating coordinate system is introduced. This system has time, position, and velocity coordinates (t, q, \dot{q}) and the rotation matrix

$$R(\omega t) = \begin{pmatrix} \cos(\omega t) & -\sin(\omega t) & 0 \\ \sin(\omega t) & \cos(\omega t) & 0 \\ 0 & 0 & 1 \end{pmatrix}. \quad (12)$$

The circular solution is $Q^*(t) = R(\omega t)q_0$, with $q_0 = (a, 0, 0)$ and $\omega = \sqrt{\mu/a^3}$.

The dynamics of the ERTBP in the uniformly rotating system require the primary and secondary masses to move in position in both the x and y directions. In order to derive the equations of motion in this system, we first introduce uniformly rotating coordinates $T_U : (t, q, \dot{q}) \rightarrow (t, Q, \dot{Q})$. Then we set $Q = R(\omega t)q$ and

$$\dot{R} = RA\omega \quad (13)$$

where

$$A = \begin{pmatrix} 0 & 1 & 0 \\ -1 & 0 & 0 \\ 0 & 0 & 0 \end{pmatrix}. \quad (14)$$

Now,

$$\ddot{Q} = R[\ddot{q} + 2\omega A\dot{q} + \omega^2 A^2 q]. \quad (15)$$

The right hand side of Equation 11 is

$$Gm_1|Q_1^* - Q|^{-3}(Q_1^* - Q) + Gm_2|Q_2^* - Q|^{-3}(Q_2^* - Q). \quad (16)$$

The elliptic solution $Q_e^*(t)$ of Kepler's equation that we use is a perturbation of the circular solution Q^* used for the CRTBP model.

$$Q_e^*(t) = R(\nu(t))r(\nu(t))Q_0^* = R(\omega t)R(\nu(t) - \omega t)q_e^*(t) \quad (17)$$

with $q_e^*(t) = r(\nu(t))Q_0^*$.

$$Q_j^* - Q = R(\omega t)[R(\nu(t) - \omega t)(q_j^* - q)] \quad (18)$$

with $q_1^* = -\mu q_e^*$ and $q_2^* = (1 - \mu)q_e^*$. The rotation matrix $R(\nu(t) - \omega t)$ compensates for the difference between the true anomaly as a function of time and the constant rotation rate. The elliptic model in uniformly rotating coordinates is

$$\ddot{q} + 2\omega A\dot{q} + \omega^2 A^2 q = R(\nu(t) - \omega t)[Gm_1 d_1^{-3}(q_1^* - q) + Gm_2 d_2^{-3}(q_2^* - q)]. \quad (19)$$

The distances are $d_1 = |q_1^* - q|$, $d_2 = |q_2^* - q|$.

Non-Uniformly Rotating ERTBP Coordinate System

We will use the true anomaly $\nu(t)$ of the solution $Q^*(t)$ to non-uniformly rotate coordinates and to keep the primary and secondary masses on the x -axis. The true anomaly will replace time as the independent variable. We use prime to denote differentiation with respect to the true anomaly. Note that even though time is replaced with true anomaly, the phase portrait of the system is still preserved. Refer to Appendix A for a description of an alternative formulation of the ERTBP in non-uniformly rotating coordinates using time as the independent variable.

The true anomaly of the solution $Q^*(t)$ satisfies the equation

$$\dot{\nu} = \sigma/r^2(\nu). \quad (20)$$

First, we define a rotation matrix

$$R(\nu) = \begin{pmatrix} \cos(\nu) & -\sin(\nu) & 0 \\ \sin(\nu) & \cos(\nu) & 0 \\ 0 & 0 & 1 \end{pmatrix}. \quad (21)$$

Then $R'(\nu) = R(\nu)A$ with

$$A = \begin{pmatrix} 0 & 1 & 0 \\ -1 & 0 & 0 \\ 0 & 0 & 0 \end{pmatrix}. \quad (22)$$

Next, introduce non-uniformly rotating coordinates $T_N : (t, X, Y) \rightarrow (t, Q, V)$, and set $Q = R(\nu(t))X$. Then $\dot{R} = R'\dot{\nu} = RA\dot{\nu}$, $\dot{Q} = R'\dot{\nu}X + R\dot{X}$. The true anomaly satisfies the conditions

$$\dot{\nu} = \sigma r^{-2}, \nu(0) = 0, \sigma = \sqrt{(Gm_1 + Gm_2)a(1 - e^2)}. \quad (23)$$

The elliptic solution $Q^*(t)$ of Kepler's equation satisfies the equation

$$Q^*(t) = R(\nu(t))r(\nu(t))Q^*(0) \quad (24)$$

where

$$r(\nu) = \frac{a(1 - e^2)}{\gamma(\nu)}, \quad \gamma(\nu) = 1 + e \cos(\nu). \quad (25)$$

In the non-uniformly rotating system the varying positions of the primary and secondary masses on the x -axis are $X_1^*(\nu(t)) = -\mu r(\nu(t))Q^*(0)$ and $X_2^*(\nu(t)) = (1 - \mu)r(\nu(t))Q^*(0)$. The equations for the ERTBP in non-uniformly rotating coordinates (ν, X, Y) are derived as follows.

$$\ddot{Q} = R[\ddot{X} + 2A\dot{\nu}\dot{X} + A\ddot{\nu}X + A^2\dot{\nu}^2X] \quad (26)$$

with $\dot{X} = X'\dot{\nu}$ and $\ddot{X} = X''\dot{\nu}^2 + X'\ddot{\nu}$. This gives the result

$$\ddot{Q} = R\dot{\nu}^2[X'' + 2AX' + A^2X] + R\ddot{\nu}[AX + X']. \quad (27)$$

Using the definition of ν we see that $\ddot{\nu} = (2\gamma'/\gamma)\dot{\nu}^2$ and $\dot{\nu}^2 = \sigma^2 r^{-4}$. Equation 26 is now

$$\ddot{Q} = R\sigma^2 r^{-4}[X'' + 2AX' + A^2X + (2\gamma'/\gamma)(AX + X')] \quad (28)$$

Express Equation 16 in terms of (ν, X) :

$$F(\nu, X) = Gm_1 \frac{RX_1^*(\nu) - RX}{r_1^3} + Gm_2 \frac{RX_2^*(\nu) - RX}{r_2^3}. \quad (29)$$

We have $r_1 = |X_1^* - X|$, $r_2 = |X_2^* - X|$, $r\sigma^{-2}Gm_1 = \gamma^{-1}(1 - \mu)$, $r\sigma^{-2}Gm_2 = \gamma^{-1}\mu$. These expressions are used to give the result that

$$F(\nu, X) = R\sigma^2 r^{-4} \left[r^3 \gamma^{-1} (1 - \mu) \frac{X_1^*(\nu) - X}{r_1^3} + r^3 \gamma^{-1} \mu \frac{X_2^*(\nu) - X}{r_2^3} \right]. \quad (30)$$

The final result is the equation

$$X'' + 2AX' + A^2X + (2\gamma'\gamma^{-1})(AX + X') = r^3 \gamma^{-1} (1 - \mu) \frac{X_1^*(\nu) - X}{r_1^3} + r^3 \gamma^{-1} \mu \frac{X_2^*(\nu) - X}{r_2^3} \quad (31)$$

with $X_1^*(\nu) = -\mu r(\nu)Q_0^*(0)$, $X_2^*(\nu) = (1 - \mu)r(\nu)Q_0^*(0)$.

For the circular problem the term $\gamma^{-1}\gamma'$ is zero, and $r = \gamma = 1$. The true anomaly and the time variables are equal in this case.

Non-Uniformly Rotating and Pulsating ERTBP Coordinate System

The derivation of the equations of motion in non-uniformly rotating, pulsating coordinates is new and uses the results for the non-uniformly rotating coordinate system. The formulas that we use in the derivation are these: $\dot{\nu} = \sigma r^{-2}$, $\ddot{\nu} = 2\phi\dot{\nu}^2$, $\gamma = 1 + e \cos(\nu)$, $\phi = \gamma^{-1}\gamma'$, $\phi' = -\phi^2 + \gamma^{-1}\gamma''$, $r = p\gamma^{-1}$, $r' = -r\phi$, $r'' = r(\phi^2 - \phi')$, $R' = RA$, $\dot{R} = R'\dot{\nu}$, $\ddot{R} = RA\dot{\nu}^2 + RA\ddot{\nu}$

Using the formulas we have $X = ru$, $X' = r(u' - \phi u)$, $X'' = -r\phi(u' - \phi u) + r(u'' - \phi'u - \phi u')$. Expanding $X'' = -r[-\phi u' + \phi^2 u + u'' + \phi^2 u - \gamma^{-1}\gamma''u - \phi u']$. After collecting terms we have

$$X'' = r[u'' + 2\phi^2 u - 2\phi u' - \gamma^{-1}\gamma''u]. \quad (32)$$

A short but key calculation shows that $[1 - \gamma^{-1}] = \gamma^{-1}\gamma''$. Replacing each of the terms on the lefthand side of Equation 31 and simplifying, the result is

$$[X'' + 2AX' + A^2X + (2\gamma'\gamma^{-1})(AX + X')] = r[u'' + 2Au' + A^2u + (1 - \gamma^{-1})u]. \quad (33)$$

Express the righthand side $F(\nu, X)$ of equation 31 in terms of (ν, u) as

$$F(\nu, X) = r^3 \gamma^{-1} (1 - \mu) \frac{X_1^*(\nu) - X}{r_1^3} + r^3 \gamma^{-1} \mu \frac{X_2^*(\nu) - X}{r_2^3} \quad (34)$$

$$F(\nu, u) = r^4 \gamma^{-1} (1 - \mu) \frac{u_1^* - u}{r_1^3} + r^4 \gamma^{-1} \mu \frac{u_2^* - u}{r_2^3} \quad (35)$$

with $u_1^* = -\mu Q^*(0)$, $u_2^* = (1 - \mu)Q^*(0)$. Note that $r_1 = rd_1 = r|u_1^* - u|$ and update. Then

$$F(\nu, u) = r[\gamma^{-1}(1 - \mu) \frac{u_1^* - u}{d_1^3} + \gamma^{-1}\mu \frac{u_2^* - u}{d_2^3}]. \quad (36)$$

The final result is

$$u'' + 2Au' + A^2u + u = (1 + e \cos(\nu))^{-1} [u + (1 - \mu)|u_1^* - u|^{-3}(u_1^* - u) + (\mu)|u_2^* - u|^{-3}(u_2^* - u)]. \quad (37)$$

The result is formulated in vector-matrix notation as follows:

$$\begin{bmatrix} x'' \\ y'' \\ z'' \end{bmatrix} + 2 \begin{bmatrix} 0 & -1 & 0 \\ 1 & 0 & 0 \\ 0 & 0 & 0 \end{bmatrix} \begin{bmatrix} x' \\ y' \\ z' \end{bmatrix} + \left(\begin{bmatrix} -1 & 0 & 0 \\ 0 & -1 & 0 \\ 0 & 0 & 0 \end{bmatrix} \begin{bmatrix} x \\ y \\ z \end{bmatrix} + \begin{bmatrix} x \\ y \\ z \end{bmatrix} \right) = \frac{1}{1 + e \cos(\nu)} \begin{bmatrix} x \\ y \\ z \end{bmatrix} + \frac{1 - \mu}{r_1^3} \left(\begin{bmatrix} -\mu \\ 0 \\ 0 \end{bmatrix} - \begin{bmatrix} x \\ y \\ z \end{bmatrix} \right) - \frac{\mu}{r_2^3} \left(\begin{bmatrix} x \\ y \\ z \end{bmatrix} - \begin{bmatrix} 1 - \mu \\ 0 \\ 0 \end{bmatrix} \right). \quad (38)$$

The equations of motion for the system may then be written in the usual form as

$$x'' = 2y' + \frac{1}{1 + e \cos(\nu)} \left[x - \frac{1 - \mu}{r_1^3} (x + \mu) - \frac{\mu}{r_2^3} (x - 1 + \mu) \right] \quad (39)$$

$$y'' = -2x' + \frac{y}{1 + e \cos(\nu)} \left[1 - \frac{1 - \mu}{r_1^3} - \frac{\mu}{r_2^3} \right] \quad (40)$$

$$z'' = -z + \frac{z}{1 + e \cos(\nu)} \left[1 - \frac{1 - \mu}{r_1^3} - \frac{\mu}{r_2^3} \right]. \quad (41)$$

The primary and secondary are fixed in this coordinate frame at $(-\mu, 0, 0)$ and $(1 - \mu, 0, 0)$, respectively.

COORDINATE SYSTEMS SUMMARY

It is often convenient to transform states and trajectories between the different ERTBP coordinate systems that we have defined so far. We will name the various coordinates as

Inertial Coordinates: Variables $(t, Q, \dot{Q}) \in R^1 \times R^3 \times R^3$

Constant Rotating Coordinates: Variables $(t, X, \dot{X}) \in R^1 \times R^3 \times R^3$

Variable Rotating Coordinates: Variables $(\nu, X, X') \in R^1 \times R^3 \times R^3$

Rotating Pulsating Coordinates: Variables $(\nu, u, u') \in R^1 \times R^3 \times R^3$

Now, we summarize the transformations between the different coordinate systems.

1. Constant Rotating to Inertial: $F : (t, X, \dot{X}) \rightarrow (t, Q, \dot{Q})$

$$Q = R(\omega t)X, \quad \dot{Q} = \dot{R}(\omega t)X + R(\omega t)\dot{X} \quad (42)$$

$$R(t) = \begin{bmatrix} \cos(\omega t) & \sin(\omega t) & 0 \\ -\sin(\omega t) & \cos(\omega t) & 0 \\ 0 & 0 & 1 \end{bmatrix} \quad (43)$$

2. Variable Rotating to Constant Rotating: $F^* : (\nu, X, X') \rightarrow (t, X, X')$

Time is expressed as a function of the true anomaly by solving the differential equation

$$\frac{dt}{d\nu} = r^2(\nu)/\sigma \quad (44)$$

with initial condition $t(0) = 0$, $\sigma = \sqrt{(Gm_1 + Gm_2)a(1 - e^2)}$, and $r(\nu) = \frac{a(1-e^2)}{1+e \cos(\nu)}$.

3. Pulsating to Variable Rotating: $G : (\nu, u, u') \rightarrow (\nu, X, X')$

$$X = u/r = \frac{1 + e \cos \nu}{1 - e^2} u \quad (45)$$

$$X' = u'/r - (u/r^2)r' \quad (46)$$

Finally, it is often convenient to convert between time and true anomaly for different formulations of the ERTBP. These conversions may be performed using Equation 44 or standard procedures which are given in Appendix B for convenience.

ILLUSTRATIVE EXAMPLE USING EVENT FUNCTIONS, POLYHEDRA, AND BISECTION

The theory of normal forms for Hamiltonian systems spans more than a century with contributions from many great mathematicians. The analysis is beautiful, complex, and difficult. It requires years of research at the highest level to understand this material. A recent publication by Jorba et al. applies state of the art normal form techniques to calculate quasi-periodic solutions of the non-autonomous bicircular problem.³⁷ While these methods yield powerful results, the methods introduced here provide an alternative that we will use to obtain similar results that apply to spacecraft mission design. These methods also lay the foundation for analyses in more complicated non-autonomous systems such as the full ephemeris model. This model may be thought of as a small perturbation of the ERTBP in systems such as the Earth-Moon, Jupiter-Europa, or Saturn-Enceladus systems among others.

To investigate the ERTBP in the vicinity of the collinear Lagrange points we use the topological concept of connectedness in combination with numerical solutions of equations of motion and event functions. In this work computer programs were used to compute exit times from regions of interest and to locate solutions that do not exit. A theoretical foundation motivating the method is based on the study of isolating blocks and the Conley index.⁵⁰

To illustrate our approach, we use a bisection method to find solutions of a non-autonomous system of differential equations that start in a specified region of phase space at a specified time and do not exit within a specified long time interval. The type of equation we use is a time-dependent vector field on R^n :

$$\dot{x} = F(t, x), x(t_0) = x_0. \quad (47)$$

An event function E_k is defined by using a base point b_k and a unit normal vector u_k .

$$E_k(x; b_k, u_k) = (x - b_k)^T u_k \quad (48)$$

The half space defined using the event function E_k is the space $H_k = \{x : E_k(x; b_k, u_k) \geq 0\}$. A polyhedron B can be viewed as the intersection of half spaces. A boundary face of B is the set $\partial_k B = B \cap \{E_k = 0\}$. A convenient event function that signals the exit of a solution from the polyhedron B is the minimum of the event functions defining the polyhedron. Our problem is to find an initial condition (t_0, x_0) in B so that the solution to the initial value problem does not exit within the time interval $[t_0, t_1]$. The behavior of the vector field in Equation 47 on the boundary

of B may be sufficient to guarantee a solution. The specific differential equation that we use as an example is given by

$$\begin{bmatrix} x_1' \\ x_2' \end{bmatrix} = \begin{bmatrix} x_1 \\ -x_2 \end{bmatrix} + \epsilon \begin{bmatrix} \cos(t)x_1 + \sin(t)x_2 \\ -\sin(t)x_1 + \cos(t)x_2 \end{bmatrix}. \quad (49)$$

The problem is to find orbits that remain in the square $B = [-1, 1] \times [-1, 1]$ for a long time. The square is defined as the intersection of four half-spaces given by four event functions. The event functions are $E_R(x) = 1 - x_1$, $E_L(x) = -1 + x_1$, $E_U(x) = 1 - x_2$, $E_D(x) = -1 + x_2$. When one of these functions is zero this indicates a right, left, up, or down exit.

The vector field in Equation 49 for $|\epsilon| < 1/\sqrt{2}$ is never tangent to the boundary of B and points outward on the right and left boundaries and inward at the top and bottom. This can be verified from the definition of the vector field. The square B is an isolating block with corners. In later, much more complicated examples the exit behaviors of solutions tangent to boundaries will be examined numerically. For this example the exit behavior of solutions to the vector field with $\epsilon = 0.6$ is illustrated for several initial start times between 0 and 2π as shown in Figure 1.

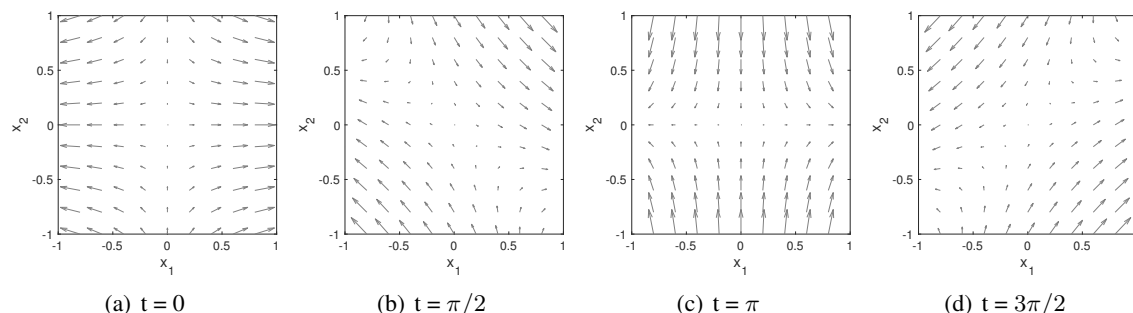


Figure 1. Vector fields for Equation 49 computed for different times.

An orbit starting in B and exiting must exit either through the right or left boundary faces. One can show that the set of initial conditions whose orbits exit right form an open set and so do the initial conditions whose orbits exit left. Given an initial time and a line segment in B with one endpoint exiting right and the other exiting left, a topological argument shows that there is a point (x_1^*, x_2^*) on that segment such that the solution of Equation 49 remains in B forward in time. The topological reason is that the line segment is a connected set, and it cannot be the union of disjoint non-empty open sets. An approximation to the point (x_1^*, x_2^*) can be found by using a bisection method together with event functions and a numerical method for solving the differential equation. It is worth noting that the bisection method will work for all small perturbations of the basic linear equation in this example. Normal form and parameterization methods generally require more work to apply than the bisection approach.

This problem was solved numerically, and the results for several cases are described next. As a first step, a line segment must be selected with end points that exit left and right. A simple case is chosen with $x_2 = 0.8$, and $-1 \leq x_1 \leq 1$. A quick check shows that the point $(-1, 0.8)$ exits left, and $(1, 0.8)$ exits right. The next step is to select an initial time for the non-autonomous system, and then a bisection method may be performed to find the value of x_1 that remains in the unit square as long as possible. (Note that this calculation is practically limited by the numerical precision of the computer.) The results for initial times $t_0 = 0$ and $t_0 + \pi/2$ are shown in Figure 2. An initial guess at $(0, 0.8)$ is shown in green in each plot, and the converged final solution from the bisection method

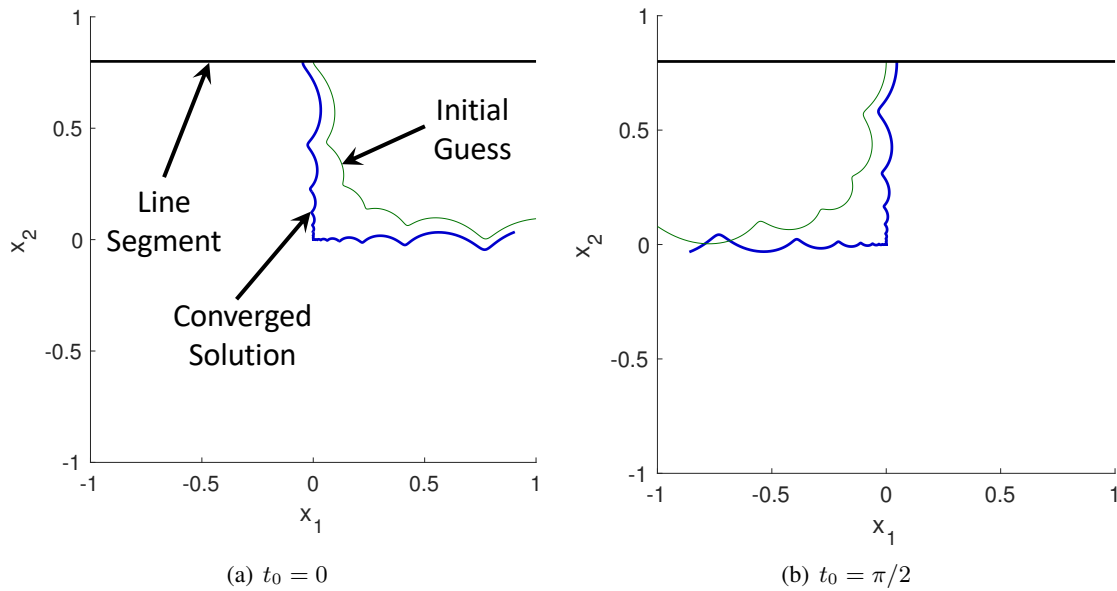


Figure 2. Converged solutions for $x_2 = 0.8$ at $t_0 = 0$ and $t_0 = \pi/2$.

is shown in blue. The converged solutions in these cases stays within the unit square for a very long time in each of these cases, but because of the limits of numerical precision of the computer, they will eventually start to wander away. The converged solutions do stay within the unit square much longer than the initial guess from the bisection method though.

ISOLATING BLOCK/NEIGHBORHOOD BOUNDARIES IN THE CRTBP AND ERTBP

In previous papers, we have explored the use of both isolating block and isolating neighborhood boundaries in the CRTBP for a variety of systems.^{6-9,51} Isolating block boundaries require that tangent trajectories immediately leave, or “bounce off” the boundaries. Isolating neighborhood boundaries are less stringent in the requirement for the test on these tangent trajectories. In this case, given “left” and “right” exit boundaries obtained in combination with the Hill’s region, the requirement is that tangent trajectories on the left boundary exit left, and tangent trajectories on the right boundary exit right. We focus on the use of isolating neighborhood boundaries here.

Cylinders were used as isolating neighborhood boundaries in Anderson, Easton, and Lo,⁸ and a similar approach is used here. As a first step, isolating neighborhood boundaries are defined and checked for the CRTBP. In this case, the inner boundary $\partial_L N$ is defined by $r_L^2 = x^2 + y^2$ where $r_L = 0.993$, and the outer boundary $\partial_R N$ is defined by $r_R^2 = (x - 1 + \mu)^2 + y^2$ where $r_R = 0.35$. In each case, the validity of the boundaries is verified for the planar problem by integrating tangent trajectories both forward and backward until they exit the isolating neighborhood. If tangent trajectories on the grid on the right side exit right and tangent trajectories on the left side exit left, this numerically verifies that the boundaries we have selected form an isolating neighborhood. Of course, this depends on the chosen grid, but by choosing a very fine grid, we expect that this procedure provides a strong argument that we have found valid boundaries. Some of the results from the integration of the tangent trajectories are illustrated in Figure 3. Here, the trajectories are integrated from the boundary until they exit a region a little larger than the boundary for easier visualization. It can be seen that the outer tangent trajectories exit the region quickly, while those

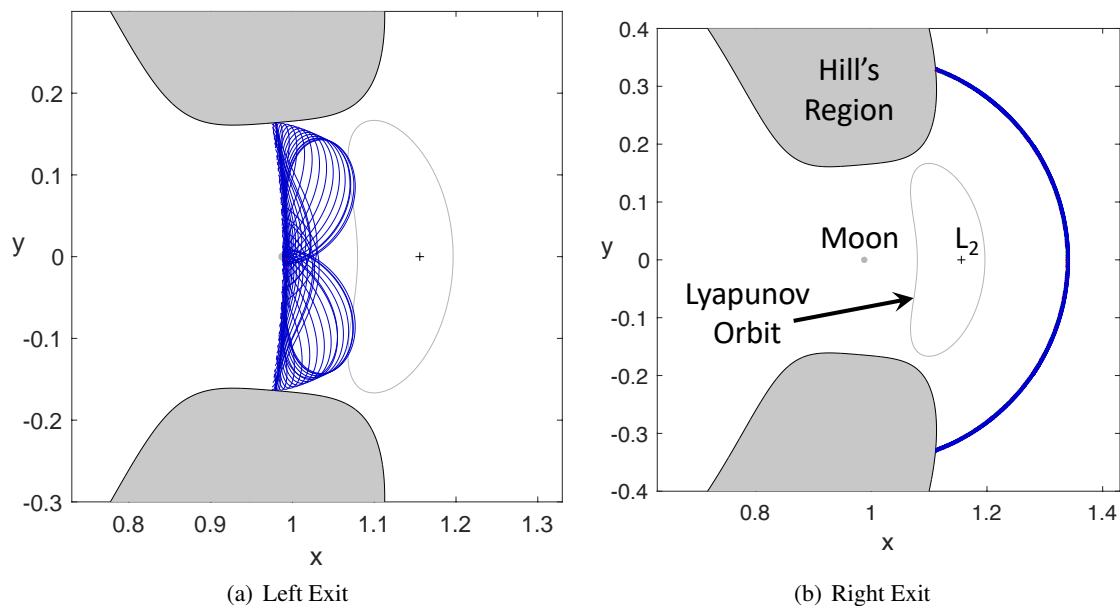


Figure 3. Test showing the tangent trajectories exiting the isolating neighborhood in the CRTBP. The L_2 Lyapunov orbit at $C = 3.10$ is shown in gray for comparison with the isolating neighborhood boundaries.

on the inner boundary wander into the isolating neighborhood before exiting left. In each case, it is verified that all tangent trajectories exit on the appropriate side.

For the autonomous CRTBP, this procedure is sufficient to check the boundaries, but for the non-autonomous ERTBP, additional computations are required. In the non-autonomous case, different tangent trajectories will be computed based on which time, or epoch, is chosen. The Jacobi constant is also no longer available to simplify the computations. Given these differences, the boundaries must be checked using tangent trajectories at a range of time spans, and a range of energies (or velocities) must also be checked. Fortunately, for the ERTBP, the system has a dimensionless period of 2π , so it is only necessary to check the boundaries on the interval from 0 to 2π before the configuration repeats. It is more difficult to determine the range of velocities or energies to check, but an instantaneous Jacobi constant may be used as a guide. This instantaneous Jacobi constant, and the equivalent Hill's region, is computed from the instantaneous state in the pulsating ERTBP frame when it is transferred to the CRTBP frame. As the state varies in the ERTBP, the equivalent Jacobi constant and Hill's region may be computed in the CRTBP, and these parameters will vary as the infinitesimal mass moves along the trajectory. This instantaneous Jacobi constant is only an approximate guide, so during subsequent calculations, trajectories crossing the isolating neighborhood boundaries are checked to verify that this assumed envelope of velocities is not violated.

We can define the tangency computations more precisely using the outer boundary as an example in the planar problem. The neighborhood boundary $\partial_R N$ can be viewed in polar coordinates as $(r, \theta, s, \phi, \nu)$ where r is the radius of the cylinder, θ gives the angular location on the cylinder, s is the speed, ϕ gives the angular direction of the velocity, and ν is the true anomaly. Here, the right exit boundary is again defined by the condition $r = 0.35$. The tangency condition is the condition $\phi = \theta \pm \pi/2$. A point $(.35, \theta_0, s, \phi_0, \nu)$ in the tangency set has two free variables; speed and true anomaly. For the CRTBP the speed is determined by the Jacobi constant, and it may be calculated

as

$$s^2 = 2\Phi(r, \theta) - 2C. \quad (50)$$

For the ERTBP, the Jacobi constant is also not constant but varies slowly, and a Jacobi function may be defined. The speed of a solution at an exit point will be close to the speed of a solution to the CRTBP at the same exit position. The Jacobi function and the associated Hill's zero velocity curve restricts the spacecraft positions in the rotating coordinate system for a fixed Jacobi constant. If an interval $[C_0, C_1]$ of Jacobi constants is used, then the smallest constant (or highest energy) determines a barrier to the positions of a solution starting from an initial condition with $J = (C_0 + C_1)/2$ and the speed satisfies the constraint

$$2\Phi(r, \theta) - 2C_0 \leq s^2 \leq 2\Phi(r, \theta) - 2C_1. \quad (51)$$

The angle θ is also constrained by the inequality $0 \leq \Phi(x, y) - C_1$. Here, a Jacobi function in polar coordinates may be defined as

$$J(t, r, \theta, s, \phi) = \frac{1}{2}s^2 - \Phi(r, \theta). \quad (52)$$

This function can provide some insight into how the Jacobi constant varies, but we have found that it is generally sufficient to use the instantaneous Jacobi constant for our numerical computations.

An additional complication is the choice of boundaries to use relative to the CRTBP boundaries in each ERTBP model. In some of the models, the positions of the primary and secondary can vary quite noticeably, making the choice of boundary locations problematic. From this perspective, the non-uniformly rotating, pulsating ERTBP model provides the easiest gateway into studying this problem. In this model, the primary and secondary remain fixed, and we may start our analysis by using fixed boundaries similar to the approach we used in the CRTBP.

An initial test using the CRTBP boundaries in the non-uniformly rotating, pulsating ERTBP revealed that the inner boundary failed the isolating neighborhood test when some of the tangent trajectories on this boundary exited right. By moving the inner boundary out to a radius of 1.02 centered on the barycenter, this problem was resolved for a range of energies or velocities. In this case, the boundaries for the ERTBP may now be defined as follows. The inner boundary $\partial_L N$ is defined by $r_L^2 = x^2 + y^2$ where $r_L = 1.02$, and the outer boundary $\partial_R N$ is defined as before by $r_R^2 = (x - 1 + \mu)^2 + y^2$ where $r_R = 0.35$. The range of required energies is defined iteratively using the instantaneous CRTBP Jacobi constant as a convenient way to parameterize energy, keeping in mind that the Jacobi constant does not exist in the ERTBP. Subsequent calculations of trajectories tracking orbits around L_2 are made, and the energy, or Jacobi constant, of trajectories intersecting the isolating neighborhood boundaries are computed. It was determined from this process that a range of Jacobi constants from 3.10 to 3.17 will be sufficient for testing the isolating neighborhood boundaries.

In order to verify that the boundaries we have selected act as isolating neighborhood boundaries under all conditions required for the orbit tracking procedure, the boundaries are tested for a range of initial dimensionless times from 0 to 2π and a range of energies, parameterized using the instantaneous CRTBP Jacobi constant, from $C = 3.10$ to 3.17. In each case, it is checked that the tangent trajectories on each boundary exit on that same boundary. The most stringent test is at the higher energy, corresponding to $C = 3.10$, and the results for this case using four different initial true anomalies are shown in Figure 4. Note that the instantaneous Hill's regions are provided for

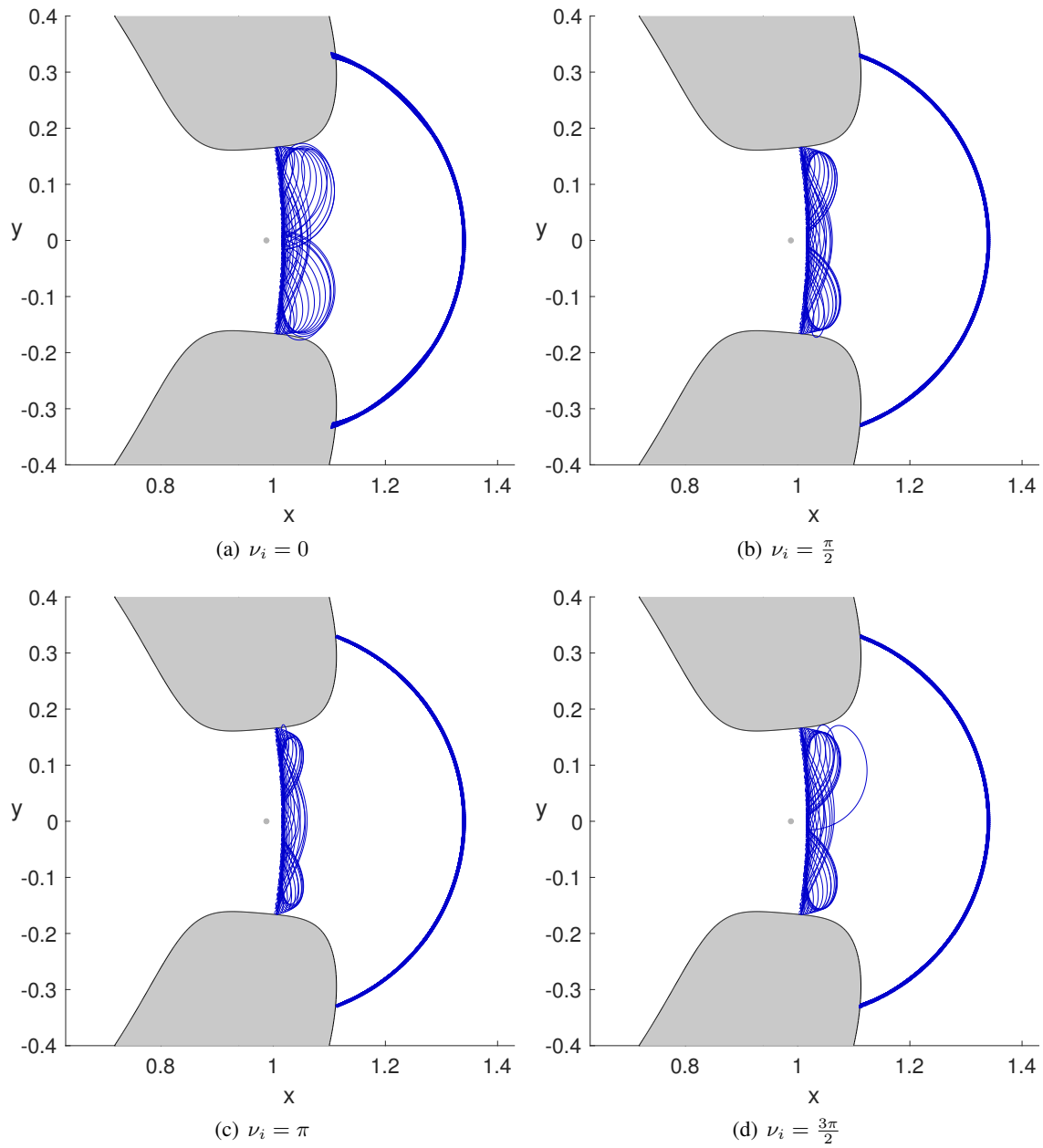


Figure 4. Test showing the tangent trajectories exiting the isolating neighborhood in the ERTBP. (The Hill's regions for the CRTBP are plotted here for comparison only.)

reference only since they do not exist in the ERTBP, and as expected, some ERTBP trajectories cross over into these regions. It can be seen from this figure that some of the trajectories on the left boundary occasionally travel into the interior before they exit left, but all tested trajectories meet the criteria. At lower energies, the trajectories generally exit from the isolating neighborhood more quickly. This result can be seen in Figure 5 where the tangent trajectories are shown for several energies for the $\nu_i = 0$ case.

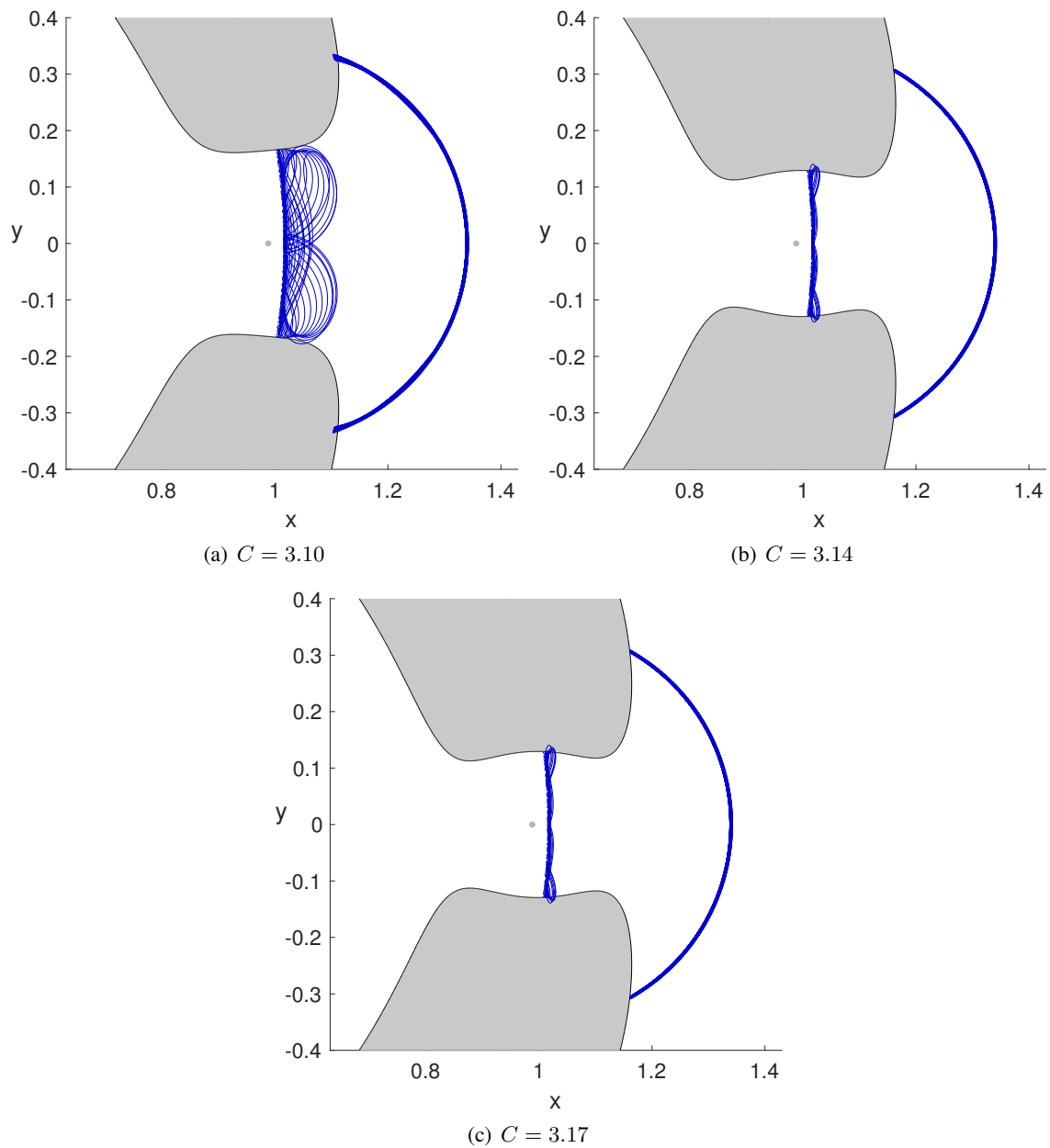


Figure 5. Test showing the tangent trajectories exiting the isolating neighborhood in the ERTBP for a range of energies with $\nu_i = 0$. (The Hill's regions for the CRTBP are plotted here for comparison only.)

ORBIT TRACKING COMPUTATIONS IN THE PLANAR ERTBP

In our previous work, we used a bisection method to compute forward asymptotic trajectories of the L_2 isolated invariant set in the CRTBP and then closely track periodic and quasiperiodic orbits.⁷ In the planar CRTBP, this produces a periodic orbit (the planar Lyapunov orbit), but in the ERTBP, we expect to compute quasiperiodic orbits using this method. As a first step, we compare with the CRTBP by selecting a base point in the CRTBP at a chosen (x, y) in the computed isolating neighborhood at $C = 3.14$. Various methods may be used as a basis for the bisection algorithm, but for this case, we compute a circle of velocities at the base point and find where they exit from the isolating neighborhood. The boundary between the sets of left and right exit trajectories in Figure 6 may be computed using bisection for the base point at $(1.16, 0.0)$. Two possible trajectories

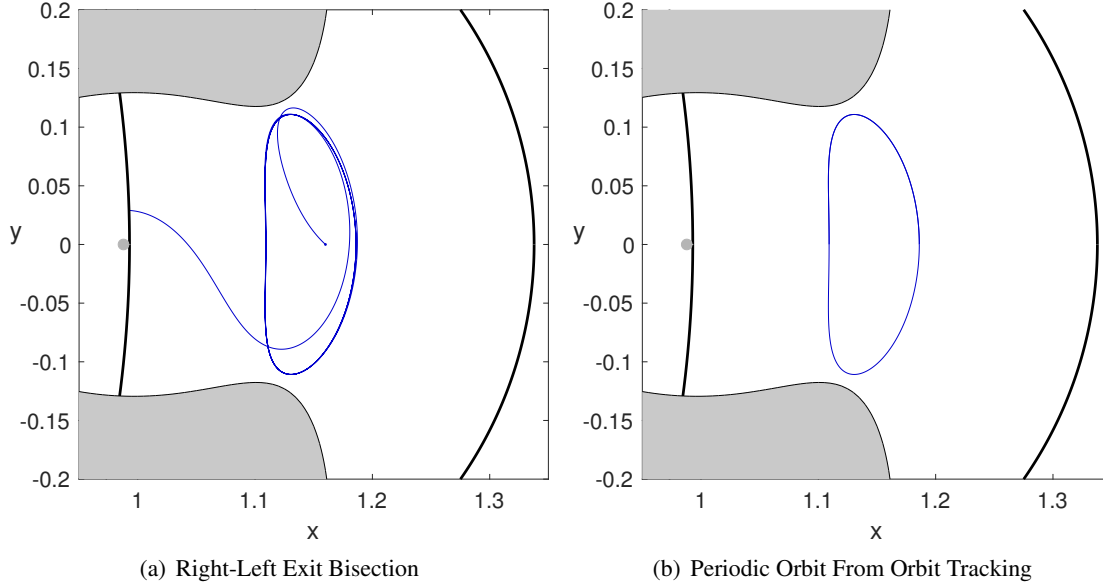


Figure 6. CRTBP forward asymptotic trajectory and quasiperiodic orbit computed for a base point at $(1.16, 0)$ with $C = 3.14$.

may be obtained which, in this case, lie on the forward asymptotic set of the L_2 isolated invariant set. Choosing one of these trajectories, and then computing corrections using the orbit tracking algorithm at each $y = 0$ crossing⁵¹ produces the trajectory in Figure 6(b) which closely tracks the L_2 Lyapunov orbit.

Now a similar procedure may be performed in the non-uniformly rotating, pulsating ERTBP model. For this case, the same base point used in the CRTBP is chosen, although it is now in a different frame. The same velocities computed in the CRTBP for $C = 3.14$ are also used at this point in the ERTBP, and a similar procedure is performed to find both the left and right exit sets along with the boundary between them. Next, one of the forward asymptotic trajectories on this boundary is selected, and an orbit tracking procedure is performed at the same $y = 0$ crossings as in the CRTBP. A slight modification is required for the ERTBP however. In the CRTBP, the Jacobi constant is used to compute the velocity at each correction, insuring that the Jacobi constant varies very little from the initial Jacobi constant. Since there is no Jacobi constant in the ERTBP, the speed that the trajectory intersects $\Sigma_{y=0}$ with is used to compute the new corrected velocity using bisection. The results from this procedure are shown in Figure 7. Note that the initial approach from the base point

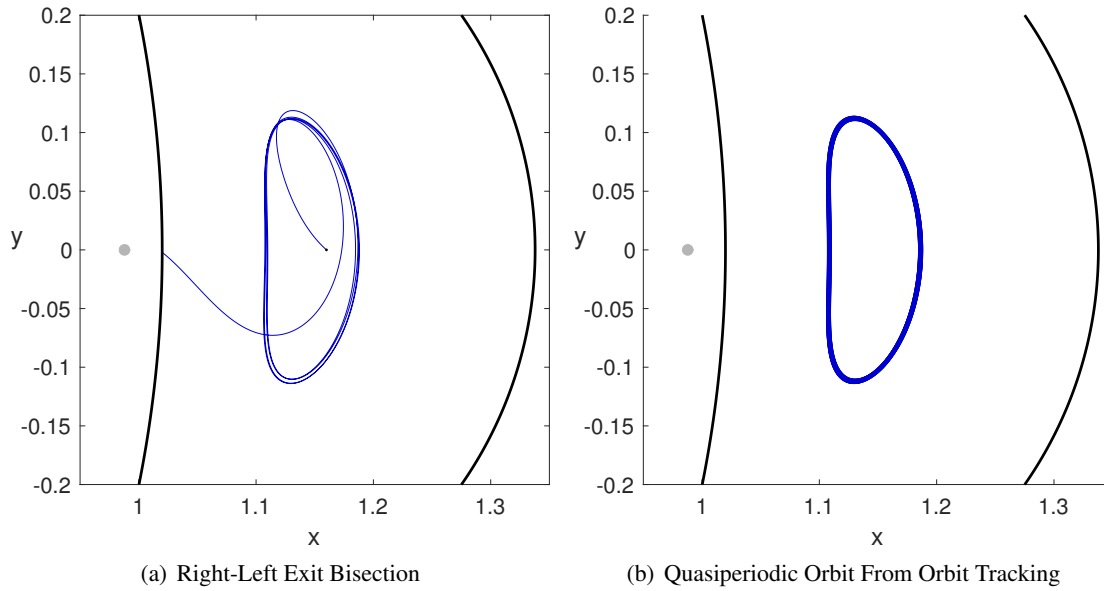


Figure 7. ERTBP forward asymptotic trajectory and quasiperiodic orbit computed for a base point at $(1.16, 0)$ with $C = 3.14$.

is shown in Figure 7(a), and only the trajectories closely tracking the quasiperiodic orbit are plotted in Figure 7(b). In this case, the computed trajectory in Figure 7(b) approaches a quasiperiodic orbit, or a 2-torus, rather than the periodic Lyapunov orbit obtained in the CRTBP. These results are in line with what would be expected in the planar ERTBP from Capinski and Zgliczyński,³³ and it is similar to results found in the bicircular problem.^{37,38,52} It is worth mentioning that some of these results require that the perturbation be sufficiently small, but our method does not specifically require this. The characteristics of the quasiperiodic orbit may be seen more clearly by plotting a Poincaré section using $\Sigma_{y=0}$ as shown in Figure 8. Now that we have implemented the algorithm

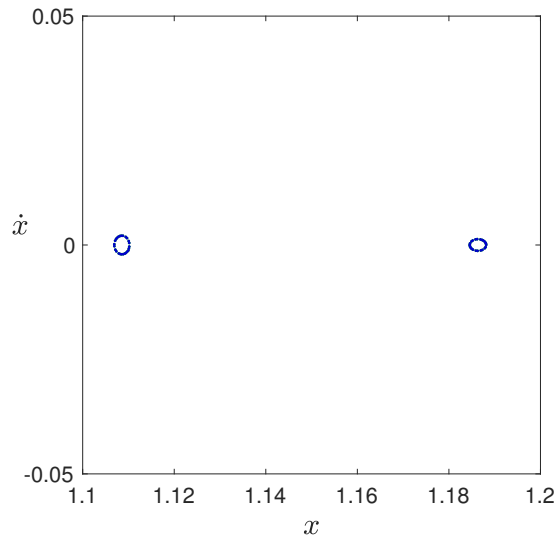


Figure 8. Intersections of the quasiperiodic orbit in Figure 7(b) with the surface of section $\Sigma_{y=0}$.

to track the quasiperiodic orbit, we next check the trajectories used in the computation to ensure that they do not go outside the range of validity of the isolating neighborhood boundaries that we have already tested. To test this, we take all of the trajectories used in the bisection portion of the orbit tracking algorithm and compute their energies, parameterized by the Jacobi constant, as they intersect the boundaries. Performing this computation gives $C_{min} \approx 3.1077$ and $C_{max} \approx 3.1675$ which is inside the range of energies when the boundaries were checked earlier.

One additional factor to include in the computation of orbits in the ERTBP is the initial epoch of the trajectory. The orbit in Figure 7 was computed for an initial epoch with $\nu_i = 0$. If a different initial epoch is chosen, a different quasiperiodic orbit will be computed. Orbits for $\nu_i = \pi/2, \pi$ are shown in Figure 9. In each case, the orbit computed at $\nu_i = 0$ is plotted in gray in the background for reference. The largest apparent difference is found for $\nu_i = \pi$.

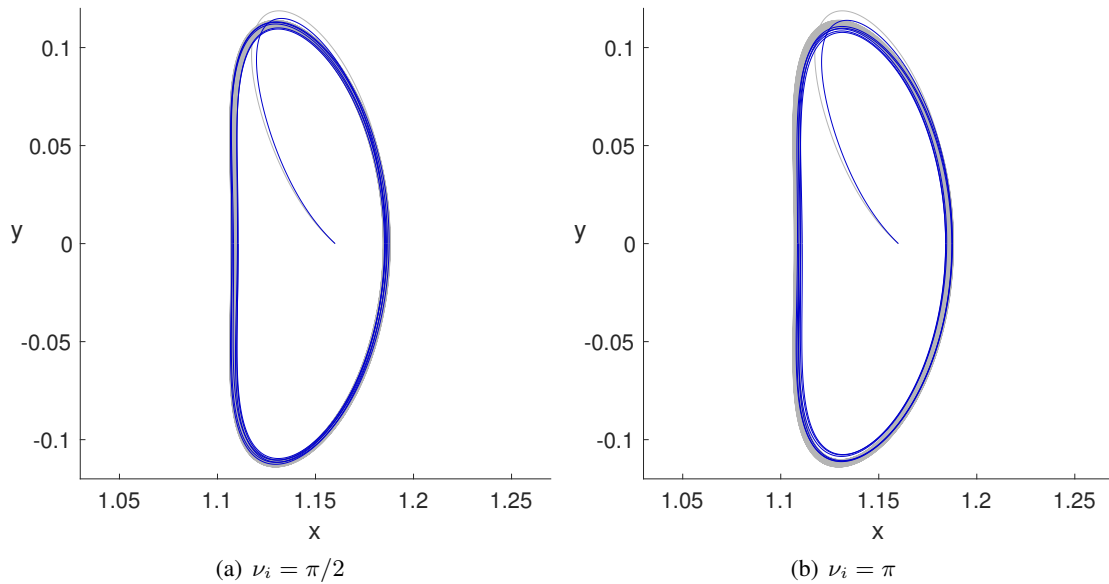


Figure 9. Quasiperiodic orbit for base point at $(1.16, 0)$ and $C = 3.14$ compute for different initial ν_i values. The gray orbit in the background was computed at $\nu_i = 0$, and it is provided for reference.

ORBIT TRACKING COMPUTATIONS IN THE SPATIAL ERTBP

The methods implemented for the planar ERTBP may be extended to the spatial ERTBP by first using cylinders rather than circles for the isolating neighborhood boundaries. The boundaries may be checked using methods very similar to those implemented in Anderson, Easton, and Lo.⁷ In brief, the checks first require the computation of a grid of points on the outer and inner cylinders. Tangent trajectories are integrated forward and backward at each of the grid points to ensure that the tangent trajectories exit on the side they started on. For the ERTBP, these conditions were checked for a range of initial times between 0 and 2π and for $3.10 \leq C \leq 3.17$ where C is once again used here as a convenient way to parameterize the velocities. The outer and inner cylinders used for $C = 3.10$ are shown relative to the Hill's region computed from the instantaneous Jacobi constant in the CRTBP in Figure 10. In this case, it is important to verify that the cylinder intersects the

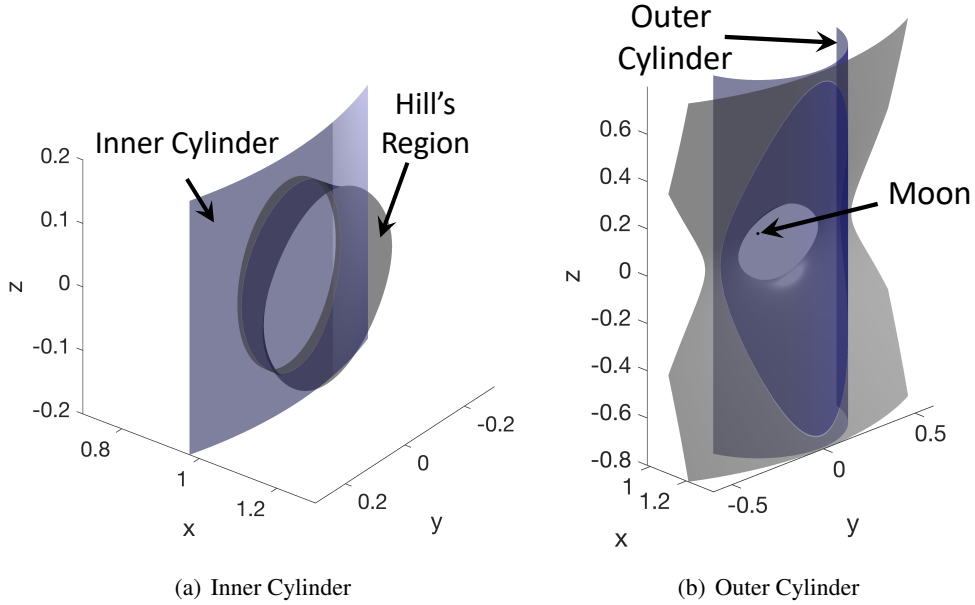


Figure 10. Schematics showing the inner and outer isolating neighborhood cylinder boundaries relative to the Hill's region for $C = 3.10$. Note that the Hill's region is computed in the CRTBP and is shown for convenience to visualize the location of the isolating neighborhood boundaries.

Hill's region at the top and the bottom.

For the spatial ERTBP the seven-dimensional phase space with coordinates $(\nu, x, y, z, x', y', z')$ and the differential Equations 39 through 41 are used for the numerical computations. A Jacobi manifold $M(C)$ is the set of all points in phase space satisfying Equation 6. The Jacobi manifolds form a layer in phase space:

$$\Lambda = \bigcup \{M(C) : 3.10 \leq C \leq 3.17\}. \quad (53)$$

The neighborhood N in phase space in which we search for quasiperiodic solutions is defined by three conditions:

$$r_L^2 = x^2 + y^2 \geq 1.02^2 \quad (54)$$

$$r_R^2 = (x + 1 - \mu)^2 + y^2 \leq .35^2, \quad (55)$$

and

$$(\nu, x, y, z, x', y', z') \in \Lambda. \quad (56)$$

As will be described next, trial solutions are generated by choosing initial conditions inside N which belong to the Jacobi manifold $M(3.14)$. In our numerical experiments we observe that these solutions do not exit the layer Λ before they exit the neighborhood N .

Once the isolating neighborhood boundaries have been checked, specific base points for computing trial solutions within the isolating neighborhood may be examined. We explore several base points here in the $z = 0$ surface of section ($\Sigma_{z=0}$), focusing on the cases where $\nu_i = 0$. We know from previous analyses in the CRTBP, that if the base point is in a region where periodic or quasiperiodic orbits exist, we can find points that stay in the isolating neighborhood forward and backward in time. The procedure for finding these points is detailed in Anderson, Easton, and Lo,⁸ but a brief summary is given here. As a first step, spheres of velocities are computed for a selected basepoint, and the velocities on these spheres that exit left and right both forward and backward in time are first computed. The boundaries of the left and right exit trajectories are computed, and their intersections contain the states that remain in the isolating neighborhood both forward and backward in time. In the ERTBP, the velocity magnitude used for the velocity spheres is chosen based upon a selected instantaneous Jacobi constant. These points are then states for trajectories contained within the isolated invariant set, and we may use them as initial conditions for tracking periodic or quasiperiodic orbits within the isolated invariant set.

Using the initial conditions computed using the intersections on the velocity sphere at a particular base point, several trajectories are integrated forward and corrected to track orbits that stay in the region. In each case, the correction is applied to the spatial orbit as it intersects $\Sigma_{z=0}$, and it compensates for the limited precision of the initial conditions and numerical integration. The correction in each case is applied to the velocity, and it is the smallest velocity correction necessary to move back to the asymptotic set. These corrections are generally very small, and specific correction magnitudes for much longer orbits will be discussed later. The selected base points are plotted in Figure 11 relative to the Lyapunov orbit computed at $C = 3.14$ in the CRTBP (plotted only for reference since our computations are in the ERTBP). Points across the region were selected so as to obtain different types of orbits corresponding to the Lissajous and quasi-halo orbits in the CRTBP.

The case with a base point at $(1.12, -0.04)$ is shown in Figure 12 with $\nu_i = 0.0$. (Unless otherwise specified all of the orbit tracking results will start with $\nu_i = 0.0$.) Here, the orbit is similar to the Lissajous orbits found in the CRTBP. Examining the intersections with $\Sigma_{z=0}$ reveals a similar topology to that found in the CRTBP, but now there are oscillations around a curve that would normally be smooth. In this case, the tori generated in the ERTBP are three-dimensional tori rather than the two-dimensional tori generated in the CRTBP.

Next, three base points were tracked in the quasi-halo region, and the results are given in Figures 13 through 15. In each case, the first portions of the quasi-halo orbits are shown so as to be able to still observe the structure in the orbits. An initial set of intersections with $\Sigma_{z=0}$ are also shown in the Poincaré sections. These base points produce three quasi-halo orbits of different sizes, and in each case the Poincaré sections show a similar overall structure to the ones observed in the CRTBP. In each case, there are also still oscillations about the expected curve.

If the orbit tracking algorithm is continued further for additional intersections with $\Sigma_{z=0}$, some additional interesting behavior may be observed for different base points. The difference in behavior between different base points was explored, and three different results are shown for base points

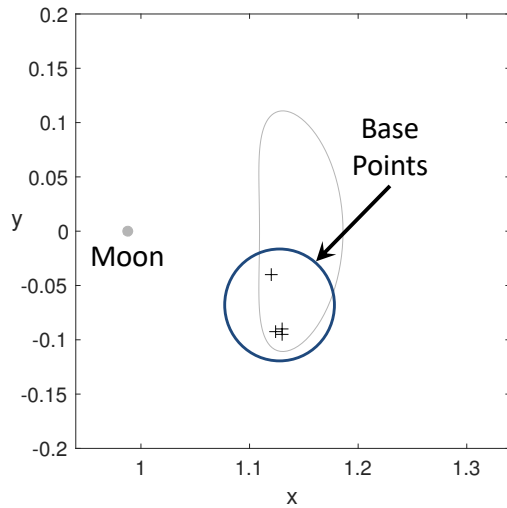


Figure 11. Overview of the base points used to track orbits in the ERTBP with $C = 3.14$. (The gray Lyapunov orbit is computed using the CRTBP and is provided for reference only.)

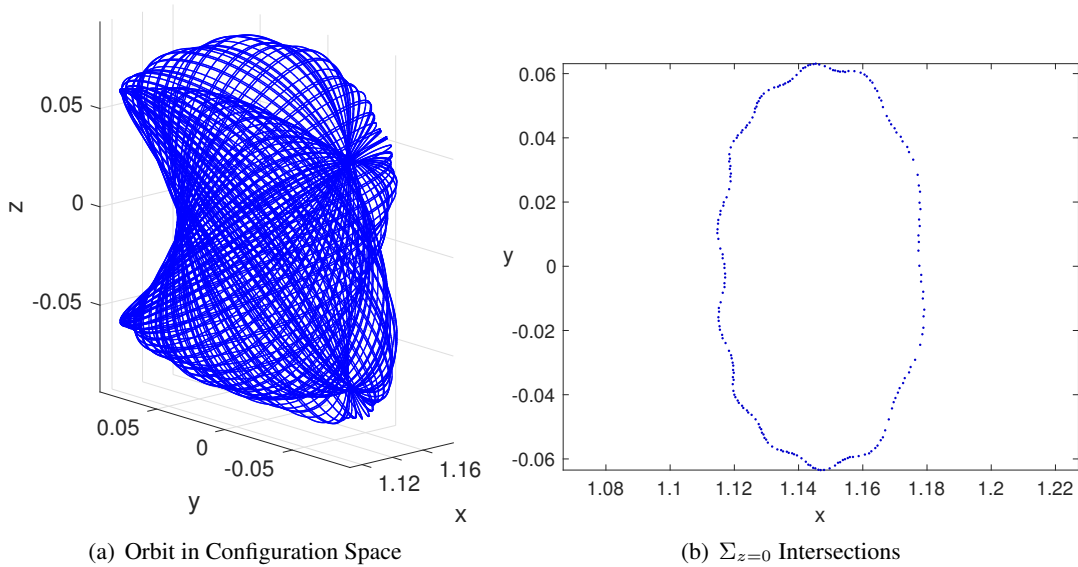


Figure 12. Quasiperiodic orbit tracked starting from base point $(1.12, -0.04)$ at $C = 3.14$.

that are relatively close in Figures 16 through 18. Some characteristics of each of these cases are compiled in Table 1. Even with over 500 revolutions, the positions are continuous, and the sum of all velocity discontinuities from the orbit tracking algorithm was always less than 6.2×10^{-5} or approximately 0.063 m/s. In each case, the initial base point was varied only slightly, but significantly different behavior was found. Note that only the portion of the Poincaré section with $x < 0$ is shown to more easily see the structure in the intersecting points. Figure 16 uses the same initial base point as Figure 13, but in this case significantly more revolutions were added. There is initial oscillatory behavior that fills in as a band as the number of revolutions is increased. If the base point location is changed slightly to $(1.130, -0.0902)$ as shown in Figure 17 then the points lie on a curve, and

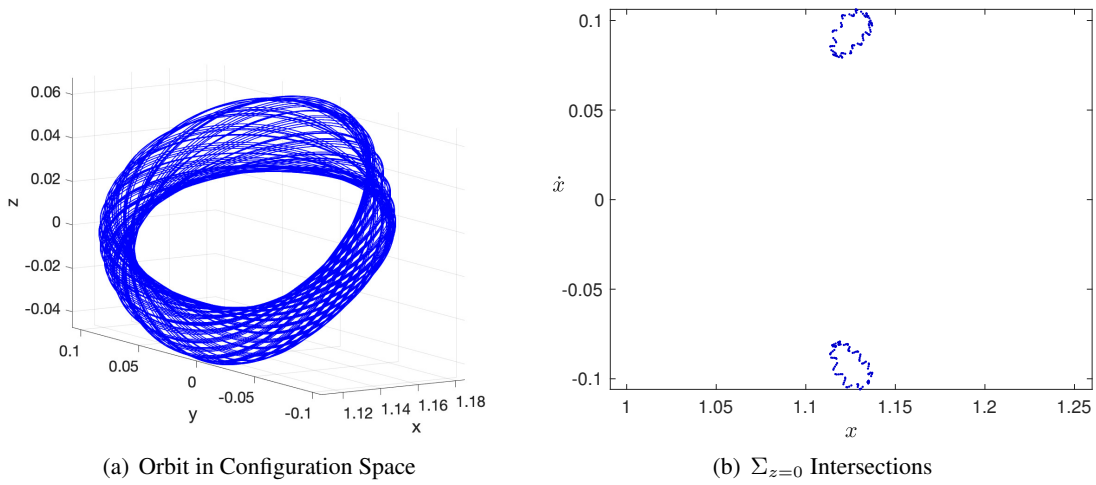


Figure 13. Quasiperiodic orbit tracked starting from base point $(1.13, -0.09)$ at $C = 3.14$.

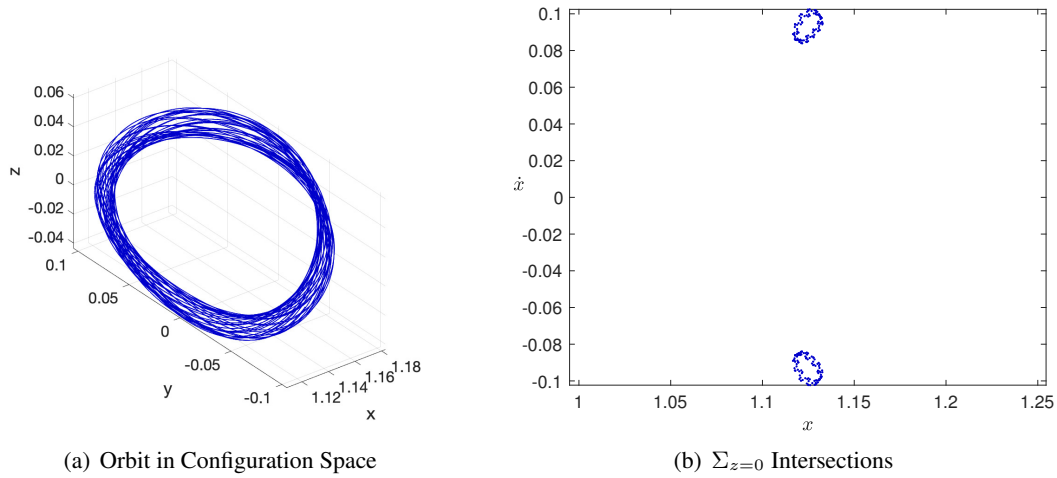


Figure 14. Quasiperiodic orbit tracked starting from base point $(1.13, -0.095)$ at $C = 3.14$.

more structure is seen in the orbit in configuration space. Finally, if another nearby base point is examined at $(1.130, -0.0902)$, as shown in Figure 18, another type of oscillatory behavior is found.

These results depend of course on the initial time that the orbit tracking algorithm is initiated, and if a different initial time is selected, then different behavior is observed. The results for a base point at $(1.130, -0.0902)$ computed with an initial time $\nu = \pi/2$ are shown in Figure 19. While the case with $\nu_i = 0$ formed a line in $\Sigma_{z=0}$, with the new initial time the intersections form a band. This result is more similar to the results using base point $(1.130, -0.0900)$ with $\nu_i = 0$, and reinforces the importance of the initial epoch in the computation of the resulting quasiperiodic orbits.

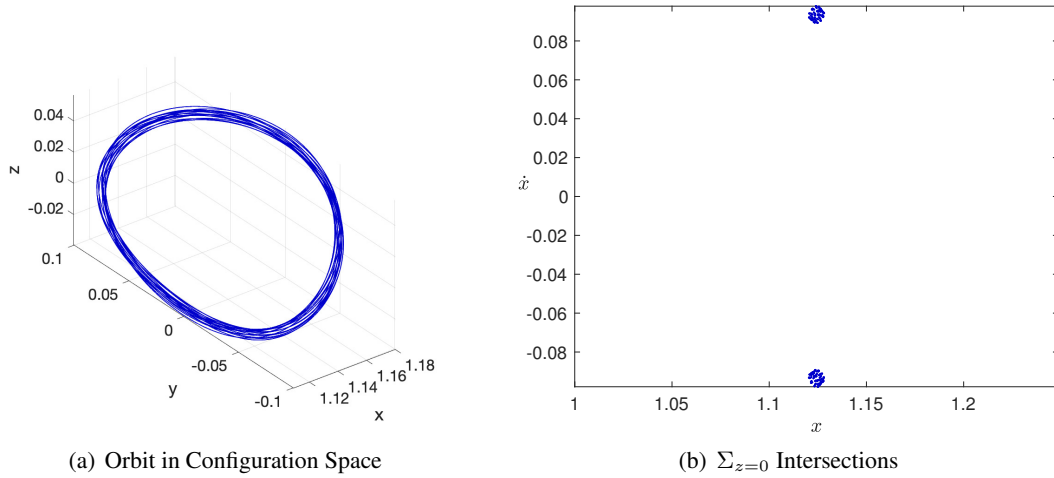


Figure 15. Quasiperiodic orbit tracked starting from base point $(1.124, -0.0925)$ at $C = 3.14$.

Table 1. Orbit tracking characteristics for large revolution orbit calculations

Base Point	Revolutions	Dimensionless Total ΔV	Dimensional Total ΔV (m/s)
$(1.130, -0.0900)$	650	6.15×10^{-5}	≈ 0.063
$(1.130, -0.0902)$	500	4.68×10^{-5}	≈ 0.048
$(1.130, -0.0903)$	500	5.43×10^{-5}	≈ 0.056

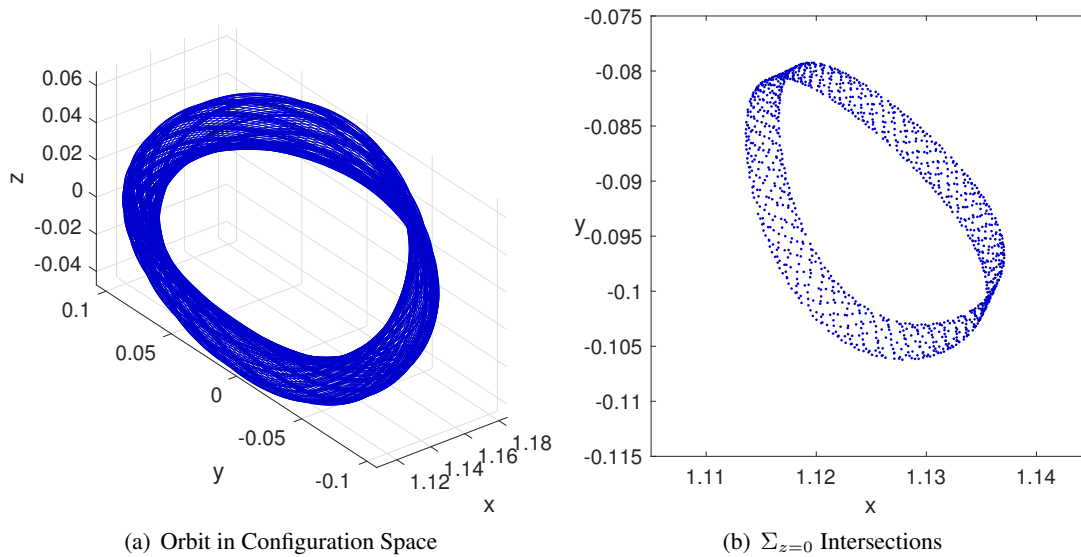


Figure 16. Quasiperiodic orbit tracked starting from base point $(1.130, -0.0900)$ with $\nu_i = 0$ at $C = 3.14$ with additional points.

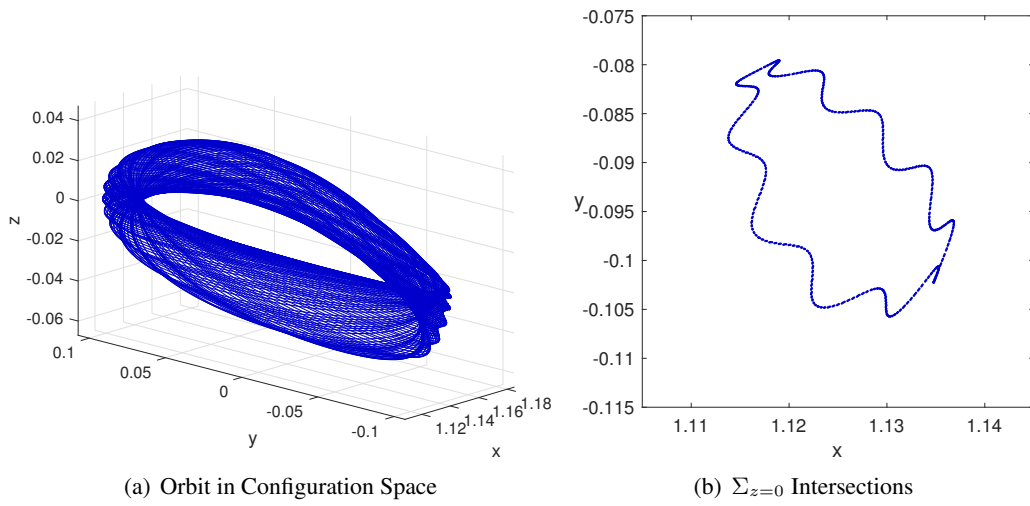


Figure 17. Quasiperiodic orbit tracked starting from base point $(1.130, -0.0902)$ at $C = 3.14$ with $\nu_i = 0$.

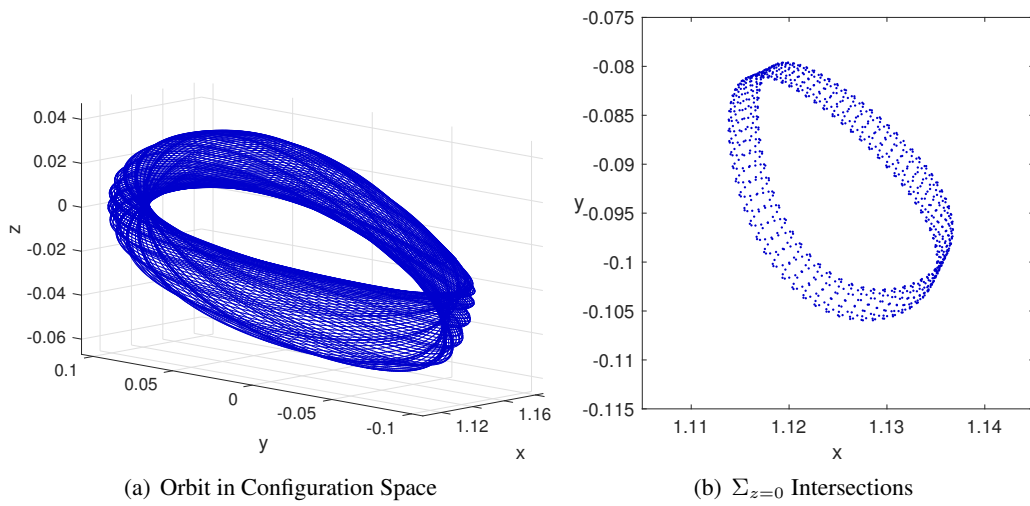


Figure 18. Quasiperiodic orbit tracked starting from base point $(1.130, -0.0903)$ at $C = 3.14$ with $\nu_i = 0$.

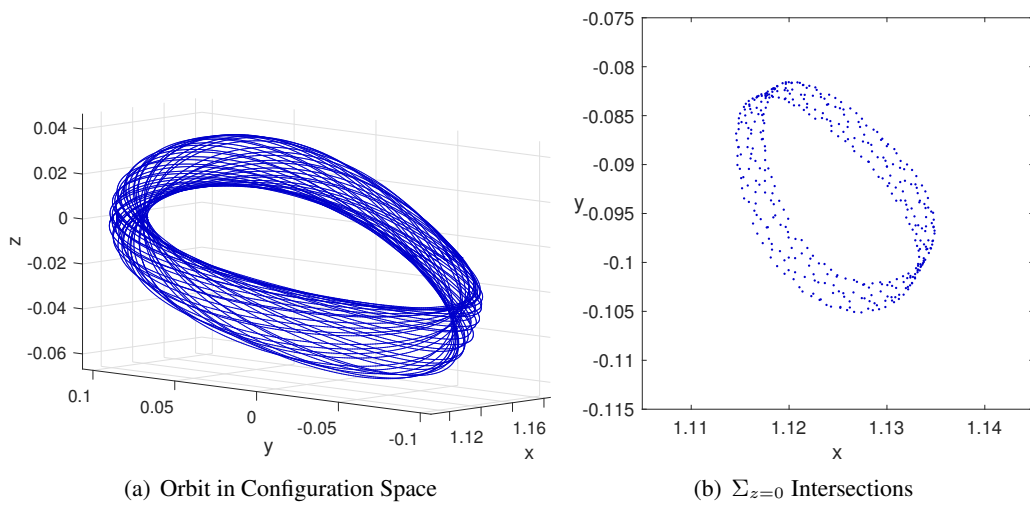


Figure 19. Quasiperiodic orbit tracked starting from base point $(1.130, -0.0902)$ at $C = 3.14$ with $\nu_i = \pi/2$.

View of Spatial Orbits in Different Coordinate Frames

In the pulsating frame, the orbits do not appear too dissimilar from the orbits computed in the CRTBP. In real-world computations, the frame is not pulsating, and it is interesting to compute these orbits in different frames. An orbit computed in the non-pulsating, variable rotating frame corresponding to the orbit in Figure 13 is shown in Figure 20. Here, the orbit still has the general

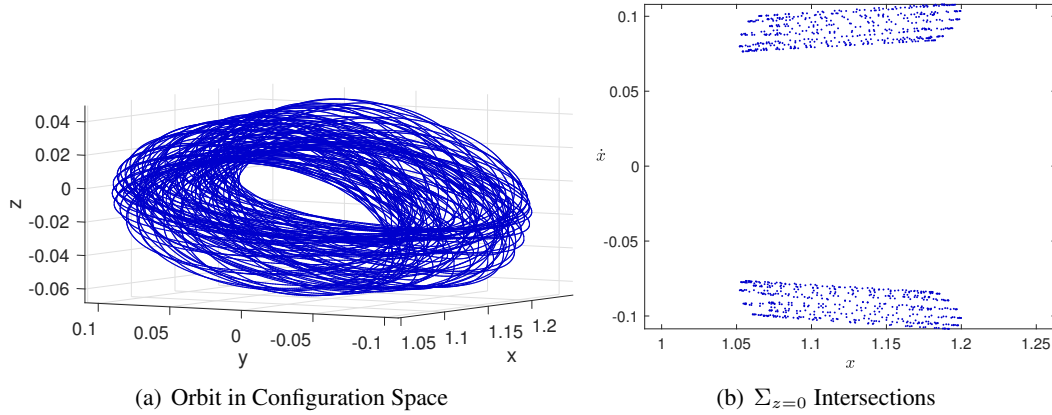


Figure 20. Quasiperiodic orbit tracked starting from base point $(1.13, -0.0902)$ at $C = 3.14$ in the variable rotating, non-pulsating frame.

characteristics of a quasi-halo orbit, but as might be expected, the orbit is elongated in the direction of the x -axis. This is easily seen in the Poincaré section shown in Figure 20(b) where the curve in Figure 17(b) is elongated as well, and structure is less easily discerned.

It is also interesting to examine the orbit in the constant rotating, non-pulsating frame equivalent to the CRTBP's rotating frame. The orbit and $\Sigma_{y=0}$ intersections are plotted in this frame in Figure 21, and some interesting characteristics may be observed. The intersections in Figure 21(b)

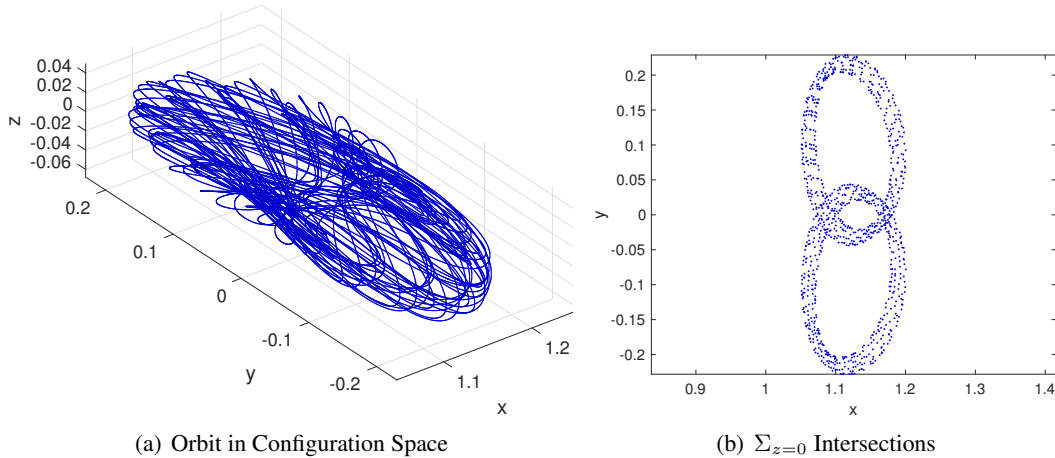


Figure 21. Quasiperiodic orbit tracked starting from base point $(1.13, -0.0902)$ at $C = 3.14$ in the constant rotating, non-pulsating frame.

now show some structure that was not apparent in the variable rotating, non-pulsating frame. As expected, the orbit also wanders further in the y direction as the frames are less aligned.

CONCLUSIONS

A method for performing isolating neighborhood computations in non-autonomous systems was developed and applied to both a simple example and the ERTBP. In the case of the simple example, it was possible to compute more stringent isolating block boundaries across all times, and in combination with a bisection method, asymptotic target trajectories that would stay within the isolating block for different initial times. In the ERTBP, it was shown that it was possible to compute isolating neighborhood boundaries that could be verified across a range of energies. By verifying that trajectories used in our orbit tracking algorithm did not go outside of this range of energies, it was found that quasiperiodic orbits around the L_2 libration point could be closely tracked in the ERTBP. Using this approach in the planar ERTBP, it was possible to compute quasiperiodic orbits, or 2-tori, equivalent to the periodic planar Lyapunov orbit in the CRTBP, and these results were found to be consistent with other results in the literature that had been found for small eccentricities. The method was successfully extended to the spatial ERTBP, and orbits equivalent to the Lissajous and quasi-halo orbits in the CRTBP were followed. In these case, these orbits had the characteristics of 3-tori, corresponding to the 2-tori in the CRTBP. Different types of behavior were observed for the quasi-halo orbits in a small region depending on the specific initial base point and initial time. The developed algorithms have now been applied in the CRTBP and ERTBP, and this approach lays the foundation for computations in other non-autonomous systems such as the bicircular and ephemeris models. This approach also allows for a relatively seamless application to these other systems with perturbations that avoids many of the difficulties inherent to other methods such as normal form or parameterization approaches.

ACKNOWLEDGEMENTS

Part of the research presented in this paper has been carried out at the Jet Propulsion Laboratory, California Institute of Technology, under a contract with the National Aeronautics and Space Administration (80NM0018D0004). This work has been supported through funding by the Multi-mission Ground System and Services Office (MGSS) in support of the development of the Advanced Multi-Mission Operations System (AMMOS).

REFERENCES

- [1] C. C. Conley, "Notes on the Restricted Three Body Problem: Approximate Behavior of Solutions Near the Collinear Lagrangian Points," Tech. Rep. TMX-53292, NASA, George C. Marshall Space Flight Center, Huntsville, Alabama, 1965.
- [2] R. W. Easton, *On the Existence of Invariant Sets Inside a Submanifold Convex to a Flow*. PhD thesis, University of Wisconsin, August 1967.
- [3] C. Conley, "Low Energy Transit Orbits in the Restricted Three-Body Problem," *SIAM Journal of Applied Mathematics*, Vol. 16, 1968, pp. 732–746.
- [4] R. W. Easton and R. McGehee, "Homoclinic Phenomena for Orbits Doubly Asymptotic to an Invariant Three-Sphere," *Indiana University Mathematics Journal*, Vol. 28, No. 2, 1979, pp. 211–240.
- [5] R. L. Anderson, R. W. Easton, and M. W. Lo, "Isolating Blocks as Computational Tools in the Circular Restricted Three-Body Problem," *Physica D: Nonlinear Phenomena*, Vol. 343, March 15 2017, pp. 38–50.
- [6] R. L. Anderson, R. W. Easton, and M. W. Lo, "Computing libration point isolated invariant sets using isolating blocks," *Physica D: Nonlinear Phenomena*, Vol. 405, April 2020.
- [7] R. L. Anderson, R. W. Easton, and M. W. Lo, "Enabling Broad Energy Range Computations at Libration Points Using Isolating Neighborhoods," *AAS/AIAA Astrodynamics Specialist Conference*, No. AAS 19-744, Portland, ME, August 11–15 2019.

- [8] R. L. Anderson, R. W. Easton, and M. W. Lo, "Direct Exploration of the L_2 Isolated Invariant Set Using Isolating Neighborhoods," *AAS/AIAA Astrodynamics Specialist Conference*, No. AAS 20-706, South Lake Tahoe, CA, August 9–13 2020.
- [9] R. L. Anderson, R. W. Easton, and M. W. Lo, "Exploration of Spatial Chaotic Orbits Using Isolating Neighborhoods," *2021 AAS/AIAA Astrodynamics Specialist Conference*, No. AAS 21-578, Big Sky, MT (Virtual), August 9–11 2021.
- [10] G. Gómez and J. M. Mondelo, "The Dynamics Around the Collinear Equilibrium Points of the RTBP," *Physica D: Nonlinear Phenomena*, Vol. 157, No. 4, 2001, pp. 283–321.
- [11] J. M. Mondelo, *Contribution to the Study of Fourier Methods for Quasi-Periodic Functions and the Vicinity of the Collinear Libration Points*. PhD thesis, Universitat de Barcelona, Barcelona, Spain, 2001.
- [12] G. Gómez, J. Masdemont, and C. Simó, "Quasihalo Orbits Associated with Libration Points," *Journal of the Astronautical Sciences*, Vol. 46, April-June 1998, pp. 135–176.
- [13] A. Haro and R. d. I. Llave, "A Parameterization Method for the Computation of Invariant Tori and their Whiskers in Quasi-Periodic Maps: Rigorous Results," *Journal of Differential Equations*, Vol. 228, 2006, pp. 530–579.
- [14] A. Haro and R. d. I. Llave, "A Parameterization Method for the Computation of Invariant Tori and Their Whiskers in Quasi-Periodic Maps: Explorations and Mechanisms for the Breakdown of Hyperbolicity," *SIAM Journal of Applied Dynamical Systems*, Vol. 6, No. 1, 2007, pp. 142–207.
- [15] A. Jorba and J. Villanueva, "Numerical Computation of Normal Forms Around Some Periodic Orbits of the Restricted Three-Body Problem," *Physica D*, Vol. 114, No. 3–4, 1998, pp. 197–229.
- [16] A. Jorba and J. Masdemont, "Dynamics in the Center Manifold of the Collinear Points of the Restricted Three Body Problem," *Physica D: Nonlinear Phenomena*, Vol. 132, No. 1–2, 1999, pp. 189 – 213.
- [17] E. Kolemen, N. J. Kasdin, and P. Gurfil, "Quasi-Periodic Orbits of the Restricted Three Body Problem Made Easy," *Proceedings of the New Trends in Astrodynamics and Applications*, August 2006.
- [18] E. Kolemen, N. J. Kasdin, and P. Gurfil, "Multiple Poincaré Sections Method for Finding the Quasiperiodic Orbits of the Restricted Three-Body Problem," *Celestial Mechanics and Dynamical Astronomy*, Vol. 112, October 2012, pp. 47–74.
- [19] Z. P. Olikara and K. C. Howell, "Computation of Quasi-Periodic Invariant Tori in the Restricted Three-Body Problem," *20th AAS/AIAA Space Flight Mechanics Meeting*, No. AAS 10-120, San Diego, California, February 2010.
- [20] Z. P. Olikara, "Computation of Quasi-Periodic Invariant Tori in the Restricted Three-Body Problem," Master's thesis, Purdue University, West Lafayette, Indiana, August 2010.
- [21] Z. P. Olikara and D. J. Scheeres, "Computing Families of Quasi-Periodic Tori in Autonomous Hamiltonian Systems," *7th European Nonlinear Dynamics Conference*, Rome, Italy, July 24-29 2011.
- [22] Z. P. Olikara and D. J. Scheeres, "Numerical Method for Computing Quasi-Periodic Orbits and Their Stability in the Restricted Three-Body Problem," *1st IAA Conference on Dynamics and Control of Space Systems*, No. IAA-AAS-DyCoSS1-08-10, Porto, Portugal, March 19-21 2012.
- [23] R. A. Broucke, "Periodic Orbits in the Restricted Three-Body Problem With Earth-Moon Masses," Technical Report 32-1168, Jet Propulsion Laboratory, February 15 1968.
- [24] R. A. Broucke, "Periodic Orbits in the Elliptic Restricted Three-Body Problem," Tech. Rep. 32-1360, Jet Propulsion Laboratory, July 15 1969.
- [25] S. Bolotin, "Second Species Periodic Orbits of the Elliptic 3 Body Problem," *Celestial Mechanics and Dynamical Astronomy*, Vol. 93, 2005, pp. 343–371.
- [26] S. Campagnola, M. Lo, and P. Newton, "Subregions of Motion and Elliptic Halo Orbits in the Elliptic Restricted Three-Body Problem," *AAS/AIAA Space Flight Mechanics Conference*, No. AAS 08-200, Galveston, Texas, January 27-31 2008.
- [27] J. M. Cors, C. Pinyol, and J. Soler, "Periodic Solutions in the Spatial Elliptic Restricted Three-Body Problem," *Physica D: Nonlinear Phenomena*, Vol. 154, No. 3-4, 2001, pp. 195 – 206.
- [28] E. Gin and P. W. Sharp, "Horseshoe Orbits for the Elliptic Restricted Three-Body Problem," Research Reports 528, University of Auckland, Department of Mathematics, Auckland, New Zealand, October 2005.
- [29] G. Gómez and M. Ollé, "A Note on the Elliptic Restricted Three-Body Problem," *Celestial Mechanics*, Vol. 39, 1986, pp. 33–55.
- [30] M. Ollé and J. R. Pacha, "The 3D elliptic restricted three-body problem: periodic orbits which bifurcate from limiting restricted problems," *Astronomy and Astrophysics*, Vol. 351, 1999, pp. 1149–1164.
- [31] D. Koh and R. L. Anderson, "Periodic Orbit-Attitude Solutions in the Planar Elliptic Restricted Three-Body Problem," *AIAA/AAS Astrodynamics Specialist Conference*, No. AAS ASD-36 2490399, Long Beach, California, September 13–16 2016.

- [32] D. Koh and R. L. Anderson, “Periodic Orbit-Attitude Solutions in the Planar Elliptic Restricted Three-Body Problem,” *Journal of Guidance, Control, and Dynamics*, Vol. 41, March 2017, pp. 644–657.
- [33] M. J. Capiński and P. Zgliczyński, “Transition Tori in the Planar Restricted Elliptic Three Body Problem,” *arXiv*, 2018.
- [34] B. Kumar, R. L. Anderson, and R. d. I. Llave, “Rapid and Accurate Computation of Invariant Tori, Manifolds, and Connections Near Mean Motion Resonances in Periodically Perturbed Planar Circular Restricted Three-Body Problem Models,” *AAS/AIAA Astrodynamics Specialist Conference*, No. AAS 20-694, South Lake Tahoe, CA, August 9–13 2020.
- [35] B. Kumar, R. L. Anderson, and R. d. I. Llave, “Rapid and accurate methods for computing whiskered tori and their manifolds in periodically perturbed planar circular restricted 3-body problems,” *Celestial Mechanics and Dynamical Astronomy*, Vol. 134, No. 3, 2022.
- [36] A. Farrés and A. Jorba, “Orbital Dynamics of a Solar Sail Near L1 and L2 in the Elliptic Hill Problem,” *63rd International Astronautical Congress*, No. IAC-12.C1.6.4, Naples, Italy, 2012.
- [37] A. Jorba, M. Jorba-Cusó, and J. J. Rosales, “The vicinity of the Earth–Moon L1 point in the bicircular problem,” *Celestial Mechanics and Dynamical Astronomy*, Vol. 132, No. 11, 2020.
- [38] J. J. Rosales, A. Jorba, and M. Jorba-Cusó, “Families of Halo-like invariant tori around L₂ in the Earth-Moon Bicircular Problem,” *Celestial Mechanics and Dynamical Astronomy*, Vol. 133, No. 16, 2021.
- [39] A. Jorba and J. Villanueva, “On the Persistence of Lower Dimensional Invariant Tori under Quasi-Periodic Perturbations,” *Journal of Nonlinear Science*, Vol. 7, 1997, pp. 427–473.
- [40] A. Fernández, A. Haro, and J. M. Mondelo, “Flow Map Parameterization Methods For Invariant Tori In Quasi-Periodic Hamiltonian Systems,” *arXiv*, 2022.
- [41] R. W. Easton, “Circular and Elliptic Restricted Three Body Problems – A Comparison,” *ArXiv*, 2021.
- [42] L. A. Hiday, *Optimal Transfers Between Libration-Point Orbits in the Elliptic Restricted Three-Body Problem*. PhD thesis, Purdue University, August 1992.
- [43] L. A. Hiday-Johnston and K. C. Howell, “Transfers Between Libration-Point Orbits in the Elliptic Restricted Problem,” *Celestial Mechanics and Dynamical Astronomy*, Vol. 58, April 1994, pp. 317–337.
- [44] K. C. Howell and L. A. Hiday-Johnston, “Time-Free Transfers Between Libration-Point Orbits in the Elliptic Restricted Problem,” *Acta Astronautica*, Vol. 32, No. 4, 1994, pp. 245–254.
- [45] V. Szebehely, *Theory of Orbits: The Restricted Problem of Three Bodies*. New York: Academic Press, 1967.
- [46] W. Scheibner, “Satz aus der Störungstheorie (Auszug aus einem Schreiben an den Herausgeber),” *Journal für die reine und angewandte Mathematik*, Vol. 65, 1866, pp. 291–292.
- [47] K. Petr and V. Nechvile, “Dvě poznámky ku speciálnímu případu problému tři těles,” *Casopis Pěstování Mat. Fys. (Praha)*, Vol. 47, 1918.
- [48] M. V. Nechvile, “Sur une nouvelle forme d’équations différentielles du problème restreint elliptique,” *Comptes rendus hebdomadaires des séances de l’Académie des sciences*, Vol. 182, 1926, pp. 310–311.
- [49] N. Rein, “Note sur l’article de M. V. Nechvil ‘sur une nouvelle forme des équations différentielles du problème restreint elliptique’,” *Trudy Gosudarstvennogo astronomicheskogo instituta im. P. K. Shternberga*, Vol. 14, No. 1, 1940, pp. 85–87.
- [50] C. Conley and R. Easton, “Isolated Invariant Sets and Isolating Blocks,” *Transactions of the American Mathematical Society*, Vol. 158, July 1971, pp. 35–61.
- [51] R. L. Anderson, R. W. Easton, and M. W. Lo, “Computing Libration Point Hyperbolic Invariant Sets Using Isolating Blocks,” *AAS/AIAA Astrodynamics Specialist Conference*, No. AAS 17-697, Stevenson, Washington, August 20-24 2017.
- [52] A. Jorba and J. Villanueva, “On the normal behaviour of partially elliptic lower-dimensional tori of Hamiltonian Systems,” *Nonlinearity*, Vol. 10, 1997, pp. 783–822.

APPENDIX

A. Non-Uniformly Rotating ERTBP Coordinate System

An alternative formulation of the ERTBP that is useful for providing insight into the problem is one where the x axis rotates non-uniformly and stays aligned with the two primaries. Given this coordinate frame, the primary and secondary will still be allowed to move along the x axis over time. Hiday and Howell⁴² define the equations of motion for this system using time as the independent variable with their notation as

$$\begin{aligned}\ddot{x} - 2n\dot{y} &= \frac{\partial U}{\partial x} + \dot{n}y \\ \ddot{y} + 2n\dot{x} &= \frac{\partial U}{\partial y} - \dot{n}x \\ \ddot{z} &= \frac{\partial U}{\partial z}\end{aligned}\tag{57}$$

where the pseudo-potential U is given by

$$U = \frac{1}{2}n^2(x^2 + y^2) + \frac{1-\mu}{r_1} + \frac{\mu}{r_2}.\tag{58}$$

Here, the variable angular velocity of the primaries is

$$n = \frac{\sqrt{1-e^2}}{(1-e\cos E)^2}\tag{59}$$

and

$$\dot{n} = -2e\frac{\sqrt{1-e^2}}{(1-e\cos E)^4}\sin E.\tag{60}$$

B. Conversion Between Time and True Anomaly

It is often convenient to convert between time and true anomaly, especially for comparing integrated trajectories given using the current ERTBP formulation and other formulations such as the one in Appendix A. Standard conversions may be used for this process.

Conversion From Time to True Anomaly: If time is the independent variable, Kepler's equation

$$M = n(t - T) = E - e \sin E\tag{61}$$

may be used to convert to ν where T is the time of periapse crossing. In this case the mean motion, $n = 1$. A Newton's method may be used to obtain E from M . Then, to obtain ν ,

$$\nu = \arccos\left(\frac{e - \cos(E)}{e \cos(E) - 1}\right)\tag{62}$$

while keeping in mind the appropriate quadrant checks.

Conversion From True Anomaly to Time: In this case, the eccentric anomaly may be computed from

$$E = \arccos\left(\frac{e + \cos(\nu)}{e \cos(\nu) + 1}\right)\tag{63}$$

while performing the appropriate quadrant checks. Then the change in time may be found using Equation 61.